TAMPEREEN TEKNILLINEN YLIOPISTO
TAMPERE UNIVERSITY OF TECHNOLOGY

PETER HEINEMANN

CORROSION PROTECTION OF MAGNESIUM ALLOYS VIA DIFFUSION COATINGS BY THE SLURRY COATING METHOD

Master of Science thesis

Examiner: Prof. Mika Valden, PD Dr. Wolfram Fürbeth
Examiner and topic approved by the Faculty Council of the Faculty of Natural Sciences
on 14th January 2015

ABSTRACT

PETER HEINEMANN: Corrosion Protection of Magnesium Alloys via Diffusion Coatings by the Slurry Coating Method
Tampere University of Technology
Master of Science thesis, 53 pages, 3 Appendix pages
June 30, 2015
Master's Degree Program in Science and Bioengineering
Major: Nanotechnology
Examiner: Prof. Mika Valden, PD Dr. Wolfram Fürbeth
Keywords: magnesium, corrosion, coating, corrosion protection, slurry coating, SEM

This thesis investigates the creation of diffusion layers by the slurry coating method using Al and Zn powders on AZ31 and AZ91. The method was applied at 450°C, 420°C and 380°C in an Ar/H_2. Secondary electron microscopy, backscattered electron microscopy, energy dispersive x-ray spectroscopy (EDX) and potentio dynamic measurements were used to classify the diffusion layers. Diffusion coatings were successfully produced at a temperature of 450°C for a Zn slurry and a mixed Al-Zn slurry. These diffusion layers were in general rich on zinc and several hundred μm thick. Electrochemical measurements showed that E_{corr} became more anodic by a zinc rich diffusion layer, but i_{corr} did not change. All in all, it could be shown that diffusion layers could be produced by the slurry coatings method for Zn and Al-Zn slurries and opportunities for further process optimisations addressed.

PREFACE

This thesis was written at the DECHEMA-Forschungsinstitute in Frankfurt am Main, Germany in the department of corrosion. The research institute provided all equipment and necessary resources. All the work related with this thesis has been done by myself and not by a third person, except all measurements related to elemental maps, linescans and their corresponding BSE images. These images were taken by the operator of the microprobe after been picked by me. Also the cross-section sample preparation has been done by metallography department. The work of this thesis includes experiments, literature research and writing.

I want to express my gratitude to the DECHEMA Forschungsinstitute for providing all the necessary space and equipment to conduct this work and Wolfram Fürbeth, as head of the working group, for the being a great help during my time here. My greatest gratitude is with Dr. Francesco Depentori for his constant help, advise and inspiring conversations. Without his help, this work could not have been completed so fast.

Furthermore, my thanks goes to all the people who helped me during this work. Gerald Schmitt for taking all the element maps and linescans. Ellen Berghof-Hasselbächer and the whole metallography for their help and advise in creating all cross-section polishes. Mathias Röhrig for his help in preparing the oven and ordering all necessary parts. Johannes Bauer for his help with all material science related questions. Antonio Pereira for his irreplacable help in preparing the electrochemical test setup and everbody I forgot, thank you for helping me with my thesis.

GLOSSARY

E^0 Electrode potential.

E_{corr} Corrosion potential.

ΔG^0 Gibbs free energy.

ρ Density of material.

F Faraday constant.

I Electrical current in ampere.

n Number of electrons.

V Polarisation during a potentio dynamic polarisation measurement..

ACRONYMS

j current density.

ADC analog digital converter.

BSE Backscattered electrons.

EC Electrochemical measurement.

EDX Energy dispersive X-ray spectroscopy.

EIS Electro impedance spectroscopy.

EMF Electro motive force.

FET field emission transistor.

MCA multichannel analyser.

OCP open circuit potential.

SE Secondary electrons.

SEM Secondary electron spectroscopy.

SHE Standard Hydrogen Electrode.

UHP Ultra-high-purity.

VE water Purified water.

TABLE OF CONTENTS

Abstract i

Preface ii

Glossary iii

Acronyms iv

1. Introduction 1

2. Theory 2

2.1 Magnesium and its alloys 2

2.1.1 Magnesium alloys 3

2.2 Corrosion and fundamentals of electrochemistry 4

2.2.1 Electrochemical cell 5

2.2.2 Galvanic corrosion 7

2.2.3 Units of corrosion 8

2.2.4 Electrical double layer 8

2.3 Corrosion characteristics of magnesium 10

2.4 Corrosion Protection 12

2.4.1 Anodic and Cathodic Protection 13

2.5 Measurement methods 14

2.5.1 Scanning electron microscopy (SEM) 14

2.5.2 Energy dispersive X-ray spectroscopy (EDX) 17

2.5.3 Electrochemical methods 18

3. Experimental 23

3.1 Thermal treatments 24

3.2 Electrochemical test setup 24

3.2.1 Corrosion testing 25

3.3 Electro Microscopy 26

4. Results 27

4.1 Characterisation of slurry powder 27
4.2 Characterisation of coatings 28
4.2.1 AZ31 28
4.2.2 AZ91 41
4.3 EC-characterisation of coatings 45
4.3.1 AZ31 45
4.3.2 AZ91 47
5. Discussion 49
6. Conclusion 52
7. Outlook 53
Bibliography 54

LIST OF FIGURES

2.1 Electrochemical cell. [15] 6

2.2 Bockris-Devanathan-Müller model 9

2.3 Potential drop along the electrical double layer[16] 10

2.4 Magnesium surface layer 12

2.5 Electrochemical force series from [16] 14

2.6 SEM Layout [25] 15

2.7 SEM scan current form 16

2.8 Electrochemical cell with three electrode setup 19

2.9 Tafel plot - Active dissolving metal 21

2.10 Anodic polarisation curve (schematic) [16] 22

3.1 Layout of the oven with example experiment setup. 23

3.2 Electrochemical cell setup 25

4.1 SE-pictures of the used Al- and Zn-powders 27

4.2 AZ31 heated at 450ï¿½C with Al-slurry for 2 hours 29

4.3 Overview of Zn-coated sample at 450ï¿½C for 2h 30

4.4 Particles with different phases at 1200x magnification 31

4.5 Sample after thorough cleaning 32

4.6 AZ31 heated at 450ï¿½C with Zn-slurry for 2 hours 33

4.7 MgO stopped diffusion process 34

4.8 AZ31 heated at 420ï¿½C with Zn-slurry 35

4.9 AZ31 heated at 450ï¿½C for 2h with an Al-Zn slurry 36

4.10 AZ31 after heat treatment at 450ï¿½C for 2h with Al-Zn slurry 37

4.11 Line scan of AZ31 at 450ï¿½C with Al-Zn slurry 38

4.12 AZ31 after heat treatment at 450ï¿½C for 1h with Al-Zn slurry 39

4.13 Different phases in the particle layer 39

4.14 AZ31 heat treated at 420ï¿½C with Al-Zn slurry 40

4.15 AZ31 after heat treatment at 380ï¿½C for 1h with Al-Zn slurry 40

4.16 AZ91 heated at 450ï¿½C with Al-slurry 41

4.17 SEM micrograph of AZ91 Al slurry coated at 420ï¿½C 42

4.18 Cross-section polish of AZ91 treated at 450ï¿½C with Zn-Slurry . . . 42

4.19 AZ91 heated at 420ï¿½C with Zn slurry 43

4.20 Diffusion layer on AZ91 after treatment with a Al-Zn slurry at 450ï¿½C 44

4.21 Analysis of AZ91 Al-slurry at 420ï¿½C 44

4.23 Corrosion measurements of AZ31 Zn coatings 46

4.24 Corrosion measurements of AZ31 AlZn coatings 46

4.25 Corrosion measurements of AZ91 Zn coatings 47

4.26 Corrosion measurements of AZ91 AlZn coatings 48

5.1 AZ31 after corrosion test 51

LIST OF TABLES

2.1 Naming scheme for magnesium alloying elements. [9] 4

2.2 Reference electrode list 19

3.1 Experiment temperatures and durations 23

3.2 Composition of applied slurries 24

3.3 Parameters for corrosion test 25

4.1 Elemental composition of the white phases in figure 4.6(a) 33

4.2 Composition of phases in figure 4.10 38

5.1 Formed phases in diffusion layers on AZ31 49

1. INTRODUCTION

Magnesium is a light metal with a density of $\rho = 1.738 \frac{g}{cm^3}$ and much lighter than iron ($\rho = 7.874 \frac{g}{cm^3}$) or aluminium ($\rho = 2.7 \frac{g}{cm^3}$). Predestinated to replace these elements, magnesium is used in the car and aerospace industry, but also for computer cases. Especially the reduced weight compared with steel or aluminium plays a big roll in making vehicles lighter and reduce their fuel intake as well as CO_2 emission. [1]

Magnesium as basic material has huge potential, but its usage is limited, due to poor corrosion performance and high chemical reactivity. The high reactivity can easily lead to corrosion in the atmosphere. The major corrosion problem of magnesium is in aqueous and chloride containing solutions, in which very high corrosion rates can be observed. [1]–[3]

In the atmosphere magnesium forms a layer of hydroxide on the surface preventing further oxidation. Nevertheless, in humid air or water the film tends to crack and exposes the pure magnesium to the corrosive environment. In general two ways of protecting magnesium parts from corrosion are followed, alloying and coating. The addition of other elements to magnesium can improve the corrosion resistance, especially aluminium and zinc are commonly used. [4]

Alloying has been proven to enhance the characteristics of magnesium and reduce the susceptibility for corrosion. Still, magnesium alloys are prone to corrosion and have to be protected by other means. Different coating processes have been developed, such as surface coversion coating, metallic coatings, organic coatings, anodizing, electroless e-coating and others. Atrens et al. [4] summarised the recent development in magnesium corrosion research and proposes a model for the corrosion of magnesium.

In the following work diffusion coatings with aluminium (Al), zinc (Zn) as well as Al-Zn were studied. The coating were applied on AZ31 and AZ91 magnesium alloys and their corrosion performance measured.

2. THEORY

This work investigates the formation of Al, Zn and Al-Zn diffusion layers on magnesium as corrosion protection layer. This chapter devided into five sections *Magnesium and its alloys*, *Corrosion and fundamentals of electrochemistry*, *Corrosion characteristics of magnesium*, *Corrosion Protection*, *Measurement methods* and provides an overview of the background knowledge for this work. In *Magnesium and its alloys* the characteristics and possibilities of alloying are explained. *Corrosion and fundamentals of electrochemistry* deals with the basic physical and chemical reactions of corrosion and link it with electrochemistry. This will be refined for the case of magnesium in section *Corrosion characteristics of magnesium* and illustrated why corrosion is such a severe problem of magnesium alloys. Means of protection against corrosion are discussed in section *Corrosion Protection* first in a general way and in detail for *anodic and cathodic protection*. The section *Measurements methodes* illustrates the fundamental mechanisms of electron microscopy, such as Secondary electrons (SE) creation, and the functional principle of a Secondary electron spectroscopy (SEM). In the end the Electrochemical measurement (EC) measurement methode used in this work, current-potential measurement, is explained.

2.1 Magnesium and its alloys

Magnesium is a light metal with an atomic mass of 24 u and with a density of 1.738 $\frac{g}{cm^3}$ much lighter than iron ($\rho = 7.874\frac{g}{cm^3}$) or aluminium ($\rho = 2.7\frac{g}{cm^3}$). It is the lightest of all metals used for constructions, has a high specific strength and can be wielded under a controlled atmosphere [1]. Nevertheless, magnesium has a few disadvantages, which are a significant problem for construction usage. The disadvantages are listed in the following [1]:

- Low elastic modulus
- Limited cold workability and toughness
- Limited high strength and creep resistance at elevated temperatures

- High chemical reactivity
- Limited corrosion resistance

In the past there has been active development on magnesium alloys, which resulted in common alloys, such as AZ31 and AZ91, with improved properties compared to crude magnesium. Especially the corrosion resistance was significantly increased. Other developed alloys are AM50 and Electron 21 [5].

2.1.1 Magnesium alloys

Magnesium can be produced by melting metallurgy and alloyed with a variety of elements. A list with the most prominent alloy elements and their effect is displayed below [6]:

Aluminium Al is the most common used alloying element and improves the cast ability and strength of alloys and limits the creep resistance.

Calcium Increase the creep resistance and roll ability of alloys.

Lithium Lithium improves the ductility, but decreases the strength of alloys. Lithium additions can further decrease the weight of magnesium alloys.

Manganese Improves the strength and, in combination with Al, reduces the solubility of Fe.

Rare Earths Rare earths increase the high temperature strength and creep resistance.

Zinc Is used together with Al and reduces the solubility of Al in Mg. The resulting precipitations increase the strength moderately. [7]

Zirconium Recent discoveries show that Zr can be used to produce Ultra-high-purity (UHP) Mg using ingot metallurgy. The resulting Mg would have a Fe content as low as $2ppm$. UHP Mg-alloys (ZX50) show a significant improved corrosion performance in 3M NaCl solution of $0.006\frac{mm}{y}$. [4]

Some elements have very detrimental effects and are considered impurities. Even very small amounts reduce the corrosion resistance significantly and must be avoided in alloys at all costs.[4]

Iron Iron is a very harmful impurity in any magnesium alloy and reduces the corrosion resistance. The content should be below $0.018\,ma\,\%$ or $180\,ppm$ [4]

Copper Similar to iron, copper reduces the corrosion resistance (upper limit $0.05\,ma\,\%$), but improves high temperature strength. [6]

Nickel Nickel is a very harmful element and greatly reduces corrosion resistance and, therefore, should be avoided as much as possible. The upper limit depends on the alloy and ranges from $5\,ppm$ for pure magnesium to $50\,ppm$ for AZ91. [8]

New research has shown that UHP Mg (Fe $< 2\,ppm$) has significantly improved corrosion resistance of as low as $0.006\frac{mm}{y}$. Silicon, usually considered as alloying element, can cause extreme corrosion rates of $100\frac{mm}{y}$ in UHP alloys. UHP alloys are still a very new, but promising research field. [4]

Similar to Al-alloys or steel, magnesium alloys have a certain naming scheme to expose the alloying elements to the reader. The naming contains in general two capital letters followed by numbers. Each letter defines one alloying element and its percentage is written behind in the respective order. In table 2.1 all alloying elements with their abbreviations are summarised.

Alloy element	Letter	Alloy element	Letter
Aluminium	A	Manganese	M
Copper	C	Silver	Q
Rare earth metals	E	Silicon	S
Thorium	H	Yttrium	Y
Zirconium	K	Zinc	Z
Lithium	L		

Table 2.1 *Naming scheme for magnesium alloying elements. [9]*

In this work AZ31 (3% Al, 1% Zn) and AZ91 (9% Al, 1% Zn) are investigated, due to their common usage by the car industry [10]. Another letter may be added after the last composition number, A etc., such as AZ 91A,B,... E. Different variants of the same alloys are described in this way. An X describes experimental alloys. [9]

2.2 Corrosion and fundamentals of electrochemistry

"Corrosion can be defined as an irreversible reaction of a material with the environment, which usually (but not always) results in a degradation of the material or its

properties." [11]

Corrosion is rather a system characteristic than a material characteristic. The same material always presents different corrosion behaviour in different environments. Magnesium may be a example here, in a dry atmosphere the surface oxide layer protects the magnesium material against further corrosion, but in a 1M NaCl solution the corrosion rate is drastically increased [2], [12], [13]. Therefore, the whole system of material and environment is very important in corrosion science and corrosion itself is a characteristic of the whole system and not a single part of it.

What reaction takes place during corrosion? Generally speaking an electrochemical redox reaction on the surface, which can be reduced to a pure electron transfer from one atom to another [11]. The basic reaction taking place on metals is:

$$M \rightarrow M^{n+} + ne^- \tag{2.1}$$

This is the oxidation. The reduction reaction depends on the environment and, as example, is in acids typically combined with hydrogen evolution

$$2H^+ + 2e^- \rightarrow H_2 \tag{2.2}$$

In aqueous solutions the oxidised metal can form a soluble cation, soluble anion or an oxide or hydroxide. General corrosion reactions of metals [11]:

$$M \rightarrow M^{n+} + ne^- \tag{2.3}$$
$$M + nH_2O \rightarrow MO_n^{m-} + 2nH^+ + (2n - m)e^- \tag{2.4}$$
$$M + nH_2O \rightarrow MO_n + 2nH^+ + 2ne^- \tag{2.5}$$
$$M + nH_2O \rightarrow M(OH)_n + nH^+ + ne^- \tag{2.6}$$

This reaction leads to the common corrosion phenomena (e.g. rust on iron) and harms the integrity of the component.

2.2.1 Electrochemical cell

An electrochemical cell consists of two half cells either connected by a salt bridge, glass frit or membrane, or mixed in each other. The ladder results in mixed potentials and was first described by Wagner and Traud in 1938 [14]. In corrosion science and especially in this work, the mixed potential theory plays a big role, due to only one physical cell (see figure 3.2). In the following first an electrochemical cell with two separated half-cells will be discussed, followed by the mixed potential theory.

Electrochemical cell with two separated half-cells

A single half cell can be considered as the corrosion of a metal in an electrolyte without connection to any other metal. The electrical connection, but not in a way that the electrolytes could mix, of two half-cells is one form of an electrochemical cell. An example with copper and zinc half-cells is shown in figure 2.1.

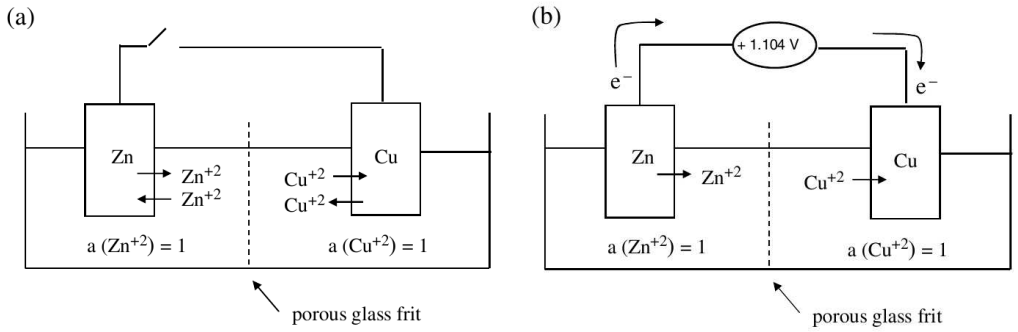

(a) Electrochemical cell with open circuit. (b) Electrochemical cell with closed circuit

Figure 2.1 *Electrochemical cell. [15]*

Figure 2.1(a) shows the equilibrium state of each cell. Important to mention here is the saturation of the electrolyte with the respective ion in a concentration to reach unit activity. Without an electrical connection each half-cell reaches an equilibrium state of oxidation and reduction, as if they would be stand alone. When the cells are electrically connected as in figure 2.1(b) the half-cell with the lower potential (vs. Standard Hydrogen Electrode (SHE)) E^0 becomes the anode and the other the cathode [15]. The resulting cell potential can be calculated by

$$E_{cell} = E_{cathode} - E_{anode} \tag{2.7}$$

with both $E_{cathode}$ and E_{anode} are the potentials of the respective electrode reduction material. All this only applies when the concentration of dissolved ions is unit activity, otherwise the half-cell potentials can be calculated using the Nernst-equation. [16]

Mixed potential theory

In a real system the two half-cells are rather one cell, than physically separated. The mixed potential theory represents a quantitative approach to a real corrosion

system, in which anodic and cathodic partial reaction constantly occur at the electrolyte/metal phase boundary. Thus, the equilibrium state would be that the total cathodic current is equal to the total anodic current. As example the reaction for Fe in acid would be:

$$|\overrightarrow{i_H}| + |\overrightarrow{i_{Fe}}| = |\overleftarrow{i_H}| + |\overleftarrow{i_{Fe}}| \tag{2.8}$$

with $\overrightarrow{i}$ as the current density of the corresponding reduction reaction and $\overleftarrow{i}$ as the current density of the respective oxidation reaction. The open circuit potential as the electrode potential of the freely corroding system is given by Eq. 2.8 and called corrosion potential E_{corr}. This potential is not related to the standard potentials of the half-cells, lies between them and is called a *mixed potential*. [16]

The corrosion current i_{corr} cannot be obtained without polarising the system, in opposition to the corrosion potential E_{corr}. Following the Wagner-Traud theory, the reduction or oxidation current densities can only be measured by polarising strongly in the anodic or cathodic direction and deduce i_{corr} from the Tafel equation. For the anodic polarisation [16]:

$$\eta_a = b_a \log \frac{\overleftarrow{i_H} + \overleftarrow{i_{Fe}}}{i_{corr}} \tag{2.9}$$

At sufficient high anodic overvoltage, so that the cathodic corrosion current is negligible, the equation can be formed into

$$\eta_a = b_a \log \frac{i}{i_{corr}} \tag{2.10}$$

i is the net anodic current density or the measured current density. A similar expression holds for the cathodic side

$$\eta_c = b_c \log \frac{i}{i_{corr}} \tag{2.11}$$

According to eq. 2.10 and eq. 2.11, $i = i_{corr}$ when $\eta = 0$. Therefore, the anodic and cathodic Tafel lines can be extrapolated to the corrosion potential E_{corr} to obtain the corrosion current density i_{corr} [16]. When using the Tafel extrapolation it must be kept in mind that it is only valid for uniform corrosion and not for localised. [16]

2.2.2 Galvanic corrosion

Galvanic corrosion occurs when two metals are physically connected in an electrolyte. A common example is a stainless steel screw in contact with a non stainless steel plate. After some time it can be observed that the plate around the screw is strongly

corroded. However, it does not only apply to macroscopic objects only, but also to microscopic impurities on the surface.

For corrosion in general it is important to know, which material is the anode and which the cathode, since the material degradation occurs at the anode. The Electro motive force (EMF) series can be used to determine the anode in an electrolyte with the material ions at unit activity. This is usually not the case for galvanic corrosion, here the ions of both metals are solved in the electrolyte. The anode and cathode of a given galvanic corrosion system can be determined by the Nernst-Equation.

2.2.3 Units of corrosion

In every science it is of uttermost importance for the reproducibility that scientists around the world use the same and thus comparable units. Especially in corrosion science this topic requires more attention than usually. Potentio dynamic polarization is a typical corrosion experiment with results given as current (I) vs. polarization (V). The current depends on the area of the metal-electrolyte interface and can be high for big electrodes and low for small electrodes for the same corrosion phenomena. An area independent unit, such as current per area or current density (j) re-establishes the comparability of experiment results. [13]

2.2.4 Electrical double layer

An important phenomenon in corrosion is the formation of an electrical double layer, when the electrode is in contact with an electrolyte. The formed double layer determines the corrosion dynamics of the whole system. Over the years several models have been developed and the Bockris-Devanathan-Mueller model is the most recent one. All models model the dynamic at the metal-solution interface.

An electrolyte is a solution of, usually, water and solved ions. Despite the charged ions and the dipole character of the water molecules the electrolyte is a non-charged liquid. There are always the same amount of anions and cations in a volume. The situation at an interface and specifically the metal-solution interface is completely different. When the metal is electrically connected with a current source, electrical charges can accumulate on the surface. Figure 2.2 illustrates the Bockris-Devanathan-Müller model of the electrical double layer at a metal-solution interface.

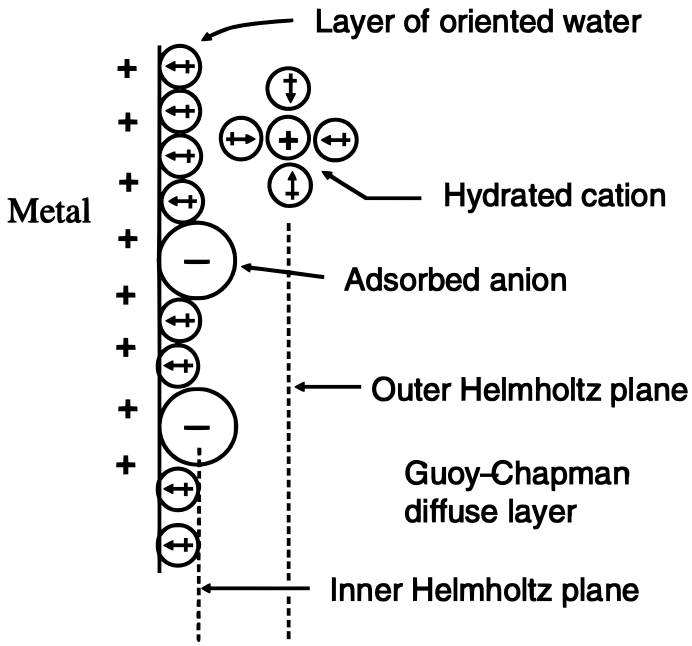

Figure 2.2 *Bockris-Devanathan-Müller model of the electrical double layer at a metal-solution interface [16]*

The model consists of three layers, the inner Helmholtz plane, the outer Helmholtz plane and the Gouy, Chapman diffuse layer. The inner Helmholtz plane consists of molecules adsorbed on the metal surface, such as ions from the electrolyte and water molecules. The outer Helmholtz plane is made of a diffuse layer of ions with the opposite charge to the ions in the inner Helmholtz plane. These ions balance the overall charge to an average zero. The third layer is the Chapman diffuse layer with ions in thermal motion. These ions are attracted by the outer Helmholtz layer, but do not increase the concentration of ions of a particular charge. [16]

During corrosion solid metal atoms are oxidised to ions and these ions solve in the electrolyte. The solving occurs because of a potential drops through the double layer from the potential of the metal to the potential of the reference electrode. Figure 2.3 illustrates this.

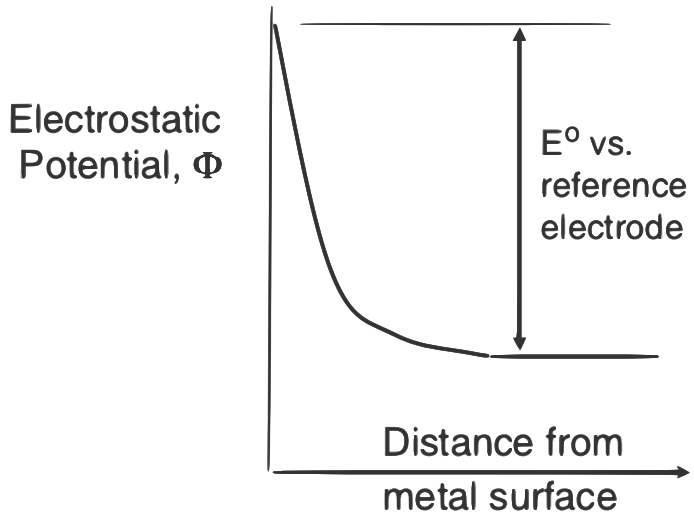

Figure 2.3 *Potential drop along the electrical double layer[16]*

The difference in potential results in a change of the free energy (see Eq. 2.12), which is the driving force for the diffusion of the ions through the double layer.

$$\Delta G^0 = -nFE^0 \tag{2.12}$$

n is the number of transferred electrons, F is the Faraday constant and E^0 the electrode potential. The value of ΔG^0 is negative and, therefore, leads to spontaneous electrochemical reactions, the transport of metal ions through the double layer. When passed through the layer the metal ions are stabilised by hydration.

2.3 Corrosion characteristics of magnesium

Magnesium is one of the most reactive metals used in construction work and usually shows severe corrosion, which limits its usage area. On the contrary magnesium samples in corrosion tests show a partially protective film and it is not uncommon that parts of the surface are unassayed even after 24h immersion in 3M NaCl solution. This example illustrates that magnesium corrosion is complex and several factors play a role in the corrosion stability of magnesium. [4]

The environment of usage plays a significant role in corrosion in general and especially for magnesium. Liu et al. [17] investigated the surface film formation on Mg and Mg-Al intermetallics and reported that pure magnesium in dry environments is protected by a stable air-formed oxide. In aqueous environments a double layer system of an inner MgO layer and an outer $Mg(OH)_2$ layer is formed. Splinter et al. [18] reported that the formed hydroxide layer cover the surface partially and grows with exposure time.

The corrosion reaction of pure magnesium consists of an anodic partial reaction, in which magnesium is oxidised and the cathodic reaction of hydrogen reduction. According to Song et al. [4] the overall and the partial reactions are:

$$2H^+ + 2e^- \rightarrow H_2 \quad (cathodic\ partial\ reaction) \tag{2.13}$$

$$2Mg \rightarrow 2Mg^+ + 2e^- \quad (anodic\ partial\ reaction) \tag{2.14}$$

$$2Mg^+ + 2H_2O \rightarrow 2Mg^{2+} + 2OH^- + H_2 \quad (water\ reaction) \tag{2.15}$$

$$Mg^{2+} + 2OH^- \rightarrow Mg(OH)_2 \quad (product\ formation) \tag{2.16}$$

$$Mg + 2H_2O \rightarrow Mg(OH)_2 + H_2 \quad (overall\ reaction) \tag{2.17}$$

In the above equations the oxidisation from $Mg- > Mg^{2+}$ is split into two one electron transfers, instead of the normal ne^- transfer. Song et al. [4], [19] suggest the formation of a uni-positive magnesium ion and its reaction with water according to the above reaction. The uni-positive ion would be produced at the magnesium surface and a part of all further reacting to Mg^{2+} and solved in the electrolyte. Shi et al. [20] illustrated the significance of this mechanism, since the apparent value valence for Mg corrosion seems to be less than 2.0 or sometimes even below 1.0. Hence, the corrosion rate extracted from Electro impedance spectroscopy (EIS) data or Tafel extrapolation is significantly lower than the corrosion rate evaluated by weight loss measurement. [4], [20], [21]

In normal atmosphere a magnesium oxide film forms on the surface of magnesium. This film is a good protection against further oxidation of the basic material, but only in a dry, halogenide free atmosphere [2], [12], [13]. Aqueous solutions containing chloride ions are a very corrosive environment for magnesium and its alloys. Today, the corrosion resistance of magnesium or alloys is often evaluated in $nM\ NaCl$ solutions, with n as high as 3.

Pure magnesium in an aqueous solution forms a partially protective surface film. Song et al. [4] states that this film has a dual layer structure of MgO and $Mg(OH)_2$. Figure 2.4 shows a schema of the dual layer with its thin ($\approx 1nm$ [4]) MgO layer in direct contact with the bare magnesium and a porous layer of $Mg(OH)_2$ on top.

Figure 2.4 *Surface dual layer structure on magnesium*

Both films are just partially protective and lead to a localised corrosion preferentially at breaks in the layers. Thus only a fraction of the overall surface undergoes corrosion.

The corrosion of magnesium alloys shows interesting difference to pure magnesium. Mathieu et al. [22] investigated the corrosion characteristic of each phase of AZ91 individually and in combination. AZ91 consists of α, β and $MnAl$ phases from which the ladder has a very limited fraction ($< 0.2\%$). Mathieu found out that the β phase is about 150mV nobler than the α phase and can act as local corrosion cathode. Zhao et al. [23] described that the β phase of AZ91 causes micro galvanic acceleration of the dissolution of the α phase and can act as a corrosion barrier if the second phase is in the form of a continuous network.

2.4 Corrosion Protection

Every material is subject to corrosion with different corrosion rates in different environments. Corrosion can never be stopped, but slowed down to technically acceptable rates. Therefore, corrosion protection deals with finding the "best material" for a certain environment. The "best material" includes a large set of attributes, such as corrosion rate, environmental friendliness, costs and many more. In this section the "best material" shall refer to the material with the least corrosion rate in a certain environment.

Corrosion protection can be achieved in various ways, painting, conversion coating, diffusion layers, anodizing, organic layers just to name a few. All protections have the same goal to shield the susceptible material against the environment with another material. The protection can be made of an artificial oxide layer or a complete

different element (e.g. zinc coating on steel). The remaining section will deal with the aspects of corrosion protection in more detail.

2.4.1 Anodic and Cathodic Protection

The overall corrosion reaction can be described as electron transfer, which results in the solution of metal atoms as ions in the electrolyte.

Many construction metals, such as steel, follow the polarisation curve in figure 2.10 and show a passivity area. Anodic polarisation utilises this material characteristic by external anodic polarisation into this area. The workpiece to be protected is connected to a potentiostate, which applies the anodic overvoltage. As result a passive oxide layer is grown on the material surface. [16]

Another way of protection is the coating of the work piece with a passive material (passive in the given corrosion environment) [16]. The coating material separates the electrolyte and the metal piece and is ideally itself immune to corrosion. In the case of cracks in the coating and exposure of the basic material to the electrolyte, the reaction depends on the potential of both materials relative to each other. If the coating is more anodic, the basic material functions as cathode and, therefore, is not attacked. In the opposite case, the area of the anode is very small compared to the cathode and a glavanic couple forms, which accelerates the corrosion. In this case the observed corrosion rates can be much higher than the anodic material alone. [16]

Other forms are “active cathodic protection with external current” and “active cathodic protection without external current”. The ladder refers to the use of sacrificial anodes to protect the working piece. A sacrificial anode is made of a material with a lower potential than the workpiece. Both are electrical connected, which enables the anodic reaction to take place on the surface of the sacrificial anode. A common material is magnesium, because of its low potential in the electrochemical series [24].

Reaction	E^0(V vs. SHE)	
$Au^{3+} + 3e^- \rightarrow Au$	+1.498	Noble
$Pt^{2+} + 2e^- \rightarrow Pt$	+1.18	↑
$Pd^{2+} + 2e^- \rightarrow Pd$	+0.951	
$Hg^{2+} + 2e^- \rightarrow Hg$	+0.851	
$Ag^{+} + e^- \rightarrow Au$	+0.800	
$Cu^{+} + e \rightarrow Cu$	+0.521	
$Cu^{2+} + 2e^- \rightarrow Cu$	+0.342	
$2H^{+} + 2e^- \rightarrow H_2$	0.000	
$Pb^{2+} + 2e^- \rightarrow Pb$	−0.126	
$Sn^{2+} + 2e^- \rightarrow Sn$	−0.138	
$Mo^{3+} + 3e^- \rightarrow Mo$	−0.200	
$Ni^{2+} + 2e^- \rightarrow Ni$	−0.257	
$Co^{2+} + 2e^- \rightarrow Co$	−0.28	
$Cd^{2+} + 2e^- \rightarrow Cd$	−0.403	
$Fe^{2+} + 2e^- \rightarrow Fe$	−0.447	
$Ga^{3+} + 3e^- \rightarrow Ga$	−0.549	
$Ta^{3+} + 3e^- \rightarrow Ta$	−0.6	
$Cr^{3+} + 3e^- \rightarrow Cr$	−0.744	
$Zn^{2+} + 2e^- \rightarrow Zn$	−0.762	
$Nb^{3+} + 3e^- \rightarrow Nb$	−1.100	
$Mn^{2+} + 2e^- \rightarrow Mn$	−1.185	
$Zr^{4+} + 4e^- \rightarrow Ze$	−1.45	
$Hf^{4+} + 4e^- \rightarrow Hf$	−1.55	
$Ti^{2+} + 2e^- \rightarrow Ti$	−1.630	
$Al^{3+} + 3e^- \rightarrow Al$	−1.662	
$U^{3+} + 3e^- \rightarrow U$	−1.798	
$Be^{2+} + 2e^- \rightarrow Be$	−1.847	
$Mg^{2+} + 2e^- \rightarrow Mg$	−2.372	
$Na^{+} + e^- \rightarrow Na$	−2.71	
$Ca^{2+} + 2e^- \rightarrow Ca$	−2.868	
$K^{+} + e^- \rightarrow K$	−2.931	↓
$Li^{+} + e^- \rightarrow Li$	−3.040	Active

Figure 2.5 *Electrochemical force series from [16]*

In "active cathodic protection with external current" the potential difference between the workpiece and the environment is compensated by an external power source. Therefore, the power source is conductively connected to the corrosive environment and the metal to be protected and compensates the corrosion current.

2.5 Measurement methods

2.5.1 Scanning electron microscopy (SEM)

The scanning electron microscope is a non-destructive method to investigate electrical conductive samples on a nanometre scale. It follows the same principle as a light microscope, that light or electrons, are used to resolve small structures and

make them visible. In a SEM an electron beam scans over the sample, interacts with it and produces secondary and backscattered electrons. These electrons carry topographical and composition information.

The operating principle of a SEM is that an electron beam is generated by an electron gun, which can be a filament (tungsten or LaB_6) or field-emission electrode. Condenser lenses are used to shape the beam and focus it into a point with a diameter of typically 10 nm or down to 1 nm for field-emission tips [25]. In figure 2.6 specimen scan coils apply a magnetic field to the electron beam and deflect it in x and y-direction.

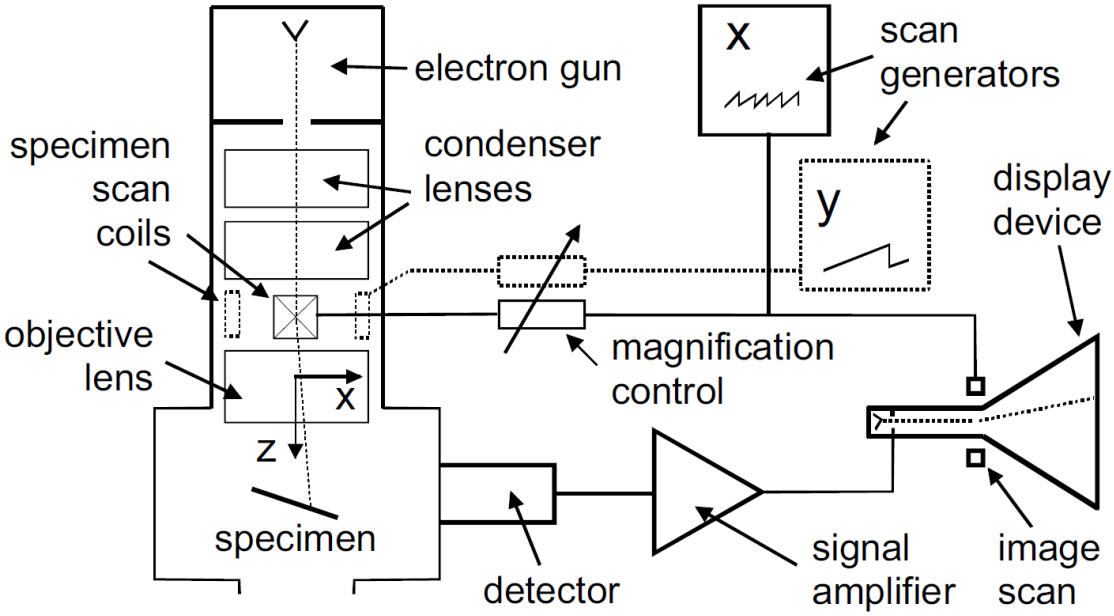

Figure 2.6 *SEM Layout [25]*

The magnetic field is generated by an oscillating saw-tooth current. Figure 2.7 displays the x- and y-direction current forms and how the picture is formed by them. (a) is the line-scan or x-direction current and (b) the frame-scan current. Through the combination of both the picture is formed as it can be seen in (d).

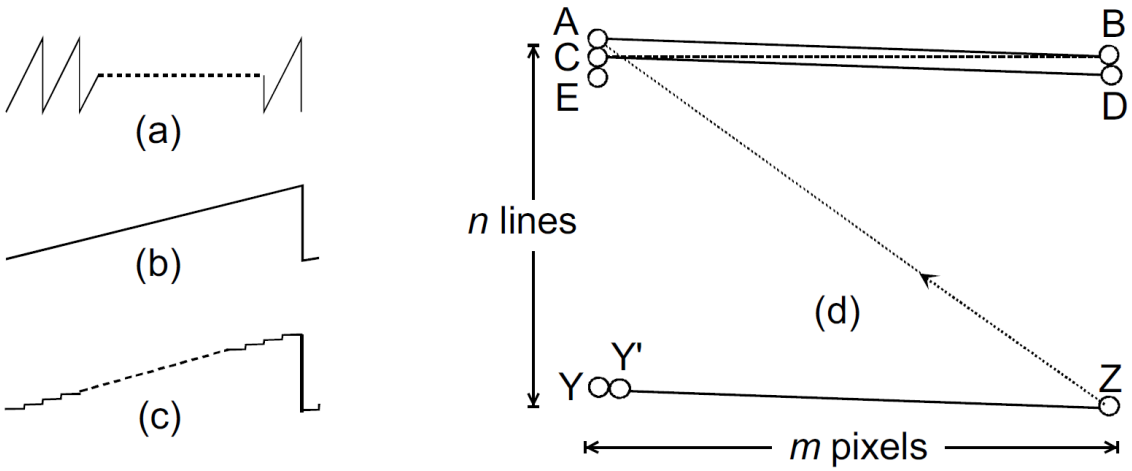

Figure 2.7 *Saw-tooth current applied to the scanning coils. (a) line-scan current, (b) frame-scan current, (c) digital frame-scan, (d) picture formation in SEM (software) [25]*

Secondary Electrons (SE)

Secondary electrons are released when the primary electrons are inelastical scattered at the atoms of the sample. When the electrons collide with the atoms some of their energy is transferred to a valence electron, which in return is released as secondary electron. One primary electron can be scattered more than one time and thus release more than one secondary electron. The ratio of secondary electrons per primary electron is called electron yield. The higher the electron yield, the better signal can be received. [25]

SE are created by inelastic scattering and, therefore, have only small amounts of kinetic energy. Thus their mean free path in a solid is short, typically a few nm, and limits the escape depth accordingly. [25] The escape depth increases with higher primary energies and measurement of very small structures can become difficult with high primary energies.

Secondary electrons are detected by an Everhart-Thornley Detector. A wire-mesh with a positive potential of several hundred volt accelerates the electrons on a scintillator, which is on a positive potential of several thousand volt. The scintillator releases about 100 photons for each incoming electron into a fibre, which guide the photons to the electron multiplier. Ladder is made of a photocathode, which converts the photons back to electrons, and dynodes. Each dynode has a potential of $100V - 200V$ with respect to the previous dynode. Each dynode multiplies incoming electrons by a factor δ and sends them to the next dynode. A serial connection of dynodes has, depending on the number n of dynodes, a high magnification. The

overall magnification of the electron multiplier depends on the electron yield and the number of the dynodes. For an electron yield of $\delta = 4$ and $n = 8$ the magnification $(\delta)^n = 10^6$. [25]

The overall electron magnification in an SEM with an electron multiplier as above and a scintillator with a photon yield of $\delta_p = 100$ is as high as $(\delta)^n_{SEM} = 10^8$. This means that each secondary electron from the sample is amplified into a current of 10^8 electrons! [25] Considering a measurement time of $10ms$ this would result in a peak current of $10nA$ by a single electron.

Backscattered Electrons

Backscattered electrons (BSE) are a second kind of electrons detected in an SEM. BSE's are elastically scattered primary electrons, which loose no or just a small amount of their energy during the scattering process. BSE and SE can be distinguished by their kinetic energy, as the BSE have a kinetic energy close to the primary electron energy. BSE can be detected like secondary electrons, but with a grid at negative potential in front of the detector to filter other electrons out.

Due to their high energy BSE come from deeper in the sample than SE. A rough estimation is half of the maximum penetration depth. [25] Therefore, BSE carry often information from several μm and not only from a few nm at the surface of the sample. Due to their high energy nature, BSE move in a straight line and are usually collect with in axis detectors.

2.5.2 EDX

When the primary electrons hit the sample, they usually interact with the weakly bounded valence electrons of the atoms. Nevertheless, there is a chance that the interaction occurs with an electron from an inner orbital. These electrons are not released due to their low energy state, but are excited to higher orbitals. Excited atom states have a short lifetime and relax fast into their ground state. During this process characteristic x-rays are emitted. It is the same principle as in an x-ray tube, just on a smaller scale. [25]

The x-rays are detected in an energy dispersive detector, which is here a semiconductor diode made from a Si single crystal. Several electrons are released when the photons enter the transition zone between the p- and n-region of the diode. Each pulse of electrons created by an x-ray photon is detected by a field emission transistor (FET)

as potential increase. Over time a step-like potential build up and analysed by a signal processor, which resets the potential of the FET. An analog digital converter (ADC) converts the signal into digital form and makes it accessible to a multichannel analyser (MCA)). The MCA reads each channel from the ADC and makes the data available to a personal computer. With the correct software the counts per photon energy is displayed. [25]

2.5.3 Electrochemical methods

Current-Potential Measurements

Current-Potential measurements are a basic tool in corrosion science to determine the extent of corrosion for a certain material in a given environment. As mentioned earlier, only the combination of material and environment validates the measurement and invest the result with significance. The measurement takes place in an electrochemical cell with a varying number of electrodes, suitable for the purpose of the measurement. The basic layout of an electrochemical cell is described in chapter 2.2. In current-potential measurements a three electrode setup is used as displayed in figure 2.8. [16]

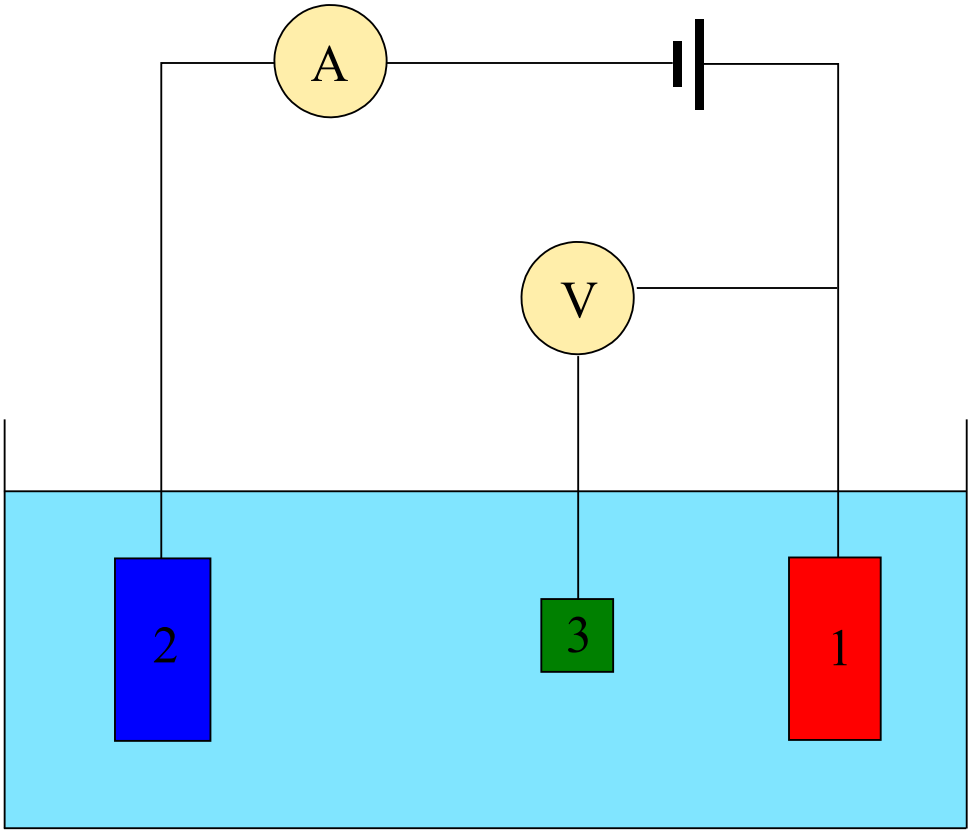

Figure 2.8 *Three electrode setup used in corrosion measurements. (1) Working electrode, (2) auxiliary electrode, (3) reference electrode [26]*

The third electrode in this setup is called *counter electrode* and keeps the reaction running. During anodic polarisation it becomes the cathode and during cathodic polarisation the anode. The potential of the counter electrode is usually not known, but which is not necessary. [27]

The reference electrode is placed a few *mm* away from the working electrode to minimise the potential drop in the electrolyte and measure the potential as local as possible. Usually the reference electrode is placed in a lugging capillary filled with a special electrolyte to minimise the interaction with the testing environment. Table 2.2 lists a few common laboratory electrodes.

Reference electrode	Electrolyte	Potential (V vs. SHE)
Saturated calomel	Saturated KCl	+0.242
Silver/silver chloride	4 M KCl with saturated AgCl	+0.222
Copper/copper sulphate	Saturated $CuSO_4$	+0.316

Table 2.2 *Reference electrodes with their electrolyte and potentials [16]*

The standard hydrogen electrode is used as zero point for all electrochemical measurements. However, the setup for this electrode is rather difficult. Therefore, other reference electrodes have been developed. The saturated calomel electrode is known and used since a long time, especially in chloride containing environments. The copper/copper sulphate is commonly used to measure potentials in the field, such as of pipelines or tanks. [16]

Current-potential measurements have a easy-to-realise setup and can provide a key values of corrosion science, the open circuit potential (OCP) or corrosion potential. The OCP is the potential emerging from the electrical double layer when a steady state is reached. Each physical system takes time to reach a steady state and the OCP can be measured as voltage between the working electrode and the reference electrode without any external polarisation. [16]

The corrosion behaviour is analysed with a current-potential measurement and is performed by polarisation relative to the OCP. A potentiostate is used to apply an external voltage between the working and reference electrode. Usually the starting point is on the cathodic side of the OCP and continues into an anodic polarisation. In magnesium corrosion research the anodic part is of uttermost interest, because it characterises the dissolution of magnesium into the electrolyte. [9], [16]

When polarising metals two different behaviours can be observed, active dissolution and an active-passive transition. Magnesium shows indications of active dissolution in chloride containing solutions [4], [9]. The typical progression of a potential dynamic measurement is depicted in figure 2.9. The material corrodes immediately and does not show any form of passivation.

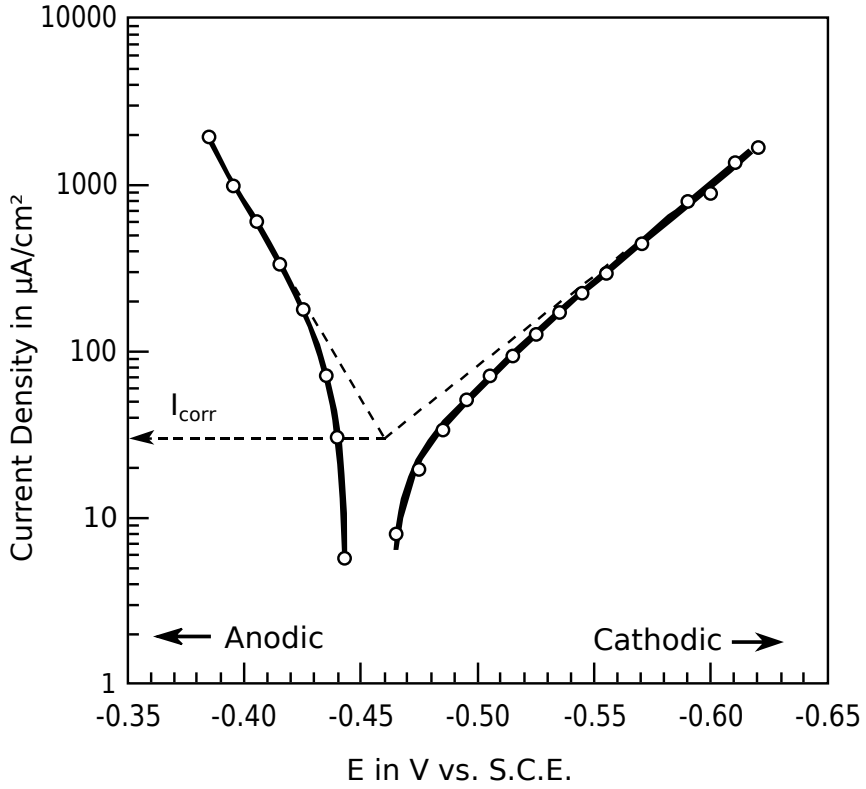

Figure 2.9 *Theoretical progression of the current density in a potentio dynamic measurement on a active dissolving metal.[28]*

In contrast to the active dissolving materials, some materials show a active-passive transition in certain environments. Stainless steel in acid as example shows a behaviour similar to those in figure 2.10. Potentio dynamic data of these materials usually shows three regions, the *active corrosion region*, the *passive region* and the *trans-passive region*. [16]

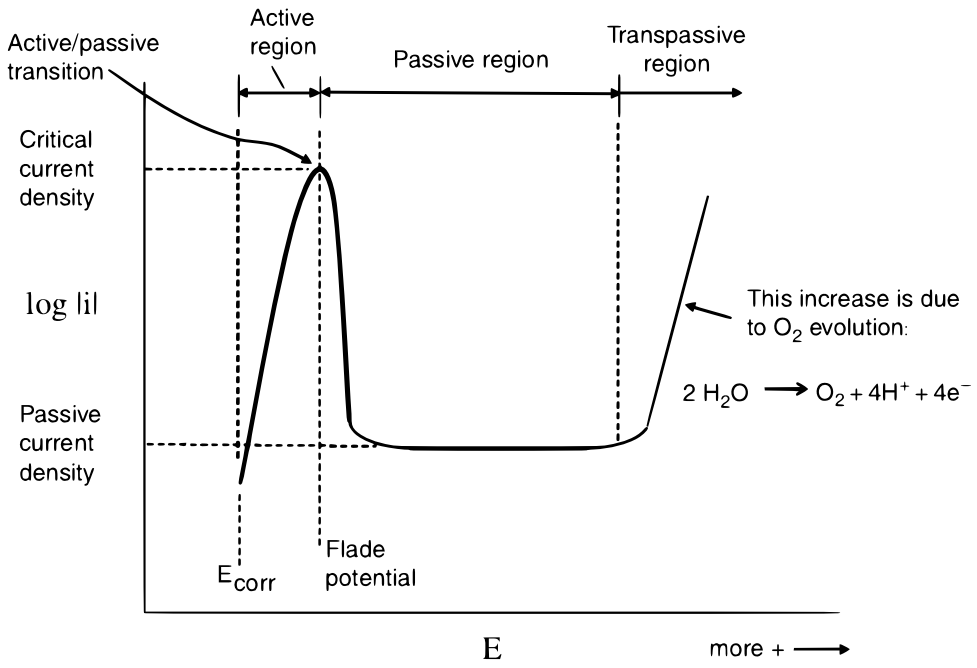

Figure 2.10 *Anodic polarisation curve (schematic) [16]*

The *active corrosion region* usually starts at $\pm 0V$ relative to the OCP and is characterised by a strong increasing corrosion current. This region ends when the current density get so high that oxides can form, which will lead to a passivation of the surface. The *flade potential* and *critical current density* are associated with this transition. Increasing the potential even further results in another steep current increase, but not due to corrosion. In the *trans-passive* region the applied potential is high enough to breakdown water into oxygen and hydrogen combined with the evolution of oxygen.

$$2H_2O(l) \rightarrow O_2(g) + 4H^+(aq) + 4e^(-) \tag{2.18}$$

3. EXPERIMENTAL

The experiments have been conducted in a tube furnace with a quartz crystal tube. Figure 3.1 shows the oven layout with quartz crystal tube, samples and titanium flakes. The samples were placed in the middle or $\frac{2}{3}$ of the tube. All experiment were carried out in an Ar/5% H_2 environment. Magnesium is a very reactive metal and reacts with even smallest amount of oxygen. Argon was chosen because of being inert and H_2 to reduce oxygen residuals or the oxide layer on magnesium. In the beginning of any experiment the tube was flushed with three times its own volume to keep oxygen residuals at a minimum. During the experiments a flow of 5-6L Ar/5% H_2 was maintained.

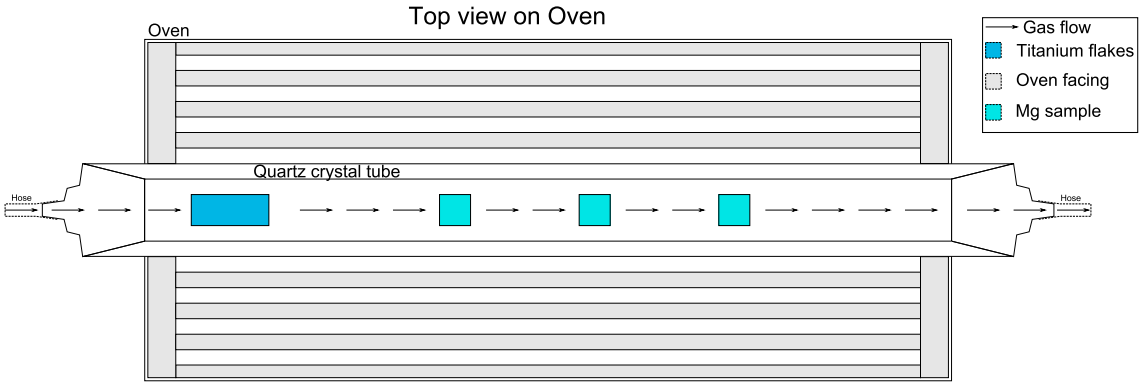

Figure 3.1 *Layout of the oven with example experiment setup.*

Three different temperatures are used in the experiments. See table 3.1 for more details.

T	450ï¿½C	420ï¿½C	380ï¿½C
t	1h, 2h	1h	1h

Table 3.1 *Experiment temperatures and durations*

The samples were prepared by ultrasonic cleaning in ethanol, followed by grinding and cleaning in Purified water (VE water) with 1000er SiC paper [4] and stored in pure ethanol. Before applying the slurries with a brush the samples were dried in

the air flow of a fume hood. Additionally the samples were exposed to air while carrying them from the preparation laboratory to the oven laboratory. This time was kept as short as possible.

3.1 Thermal treatments

The corrosion protection coatings are produced by the slurry coating method. Therefore, slurry made of terpineol, made viscous with cellulose, was mixed with different metal particles and applied on samples. The basic slurry was made of terpineol, in which cellulose was added. The mixing was performed by adding two steel balls into the container and roll it for several hours. The final slurries used in the experiments were made in a 3-step process, the single steps are:

1. Weigh the terpineol and metal powder(s)
2. Mix them by hand with a spatula
3. Fine mixing with a roll mill

The slurries used in this work are listed below.

Table 3.2 *Composition of applied slurries*

Slurry	Terpineol [wt.%]	Aluminium [wt.%]	Zinc [wt.%]
S1	50	25	25
S2	50	50	0
S3	50	0	50

3.2 Electrochemical test setup

All electrochemical tests have been performed with a PGP201 potentiostate from Radiometer Copenhagen in an electrochemical cell with a three electrode setup. The software used for controlling the experiments was VoltaMaster 4 in Version 7.8. Figure 3.2 shows the layout of the cell with the working electrode, the reference electrode and the counter electrode. The Mg-sample is pressed against the bottom of the cell and electrically connected through a copper pin. In the experiments only one side of the sample is coated and put into contact with the electrolyte.

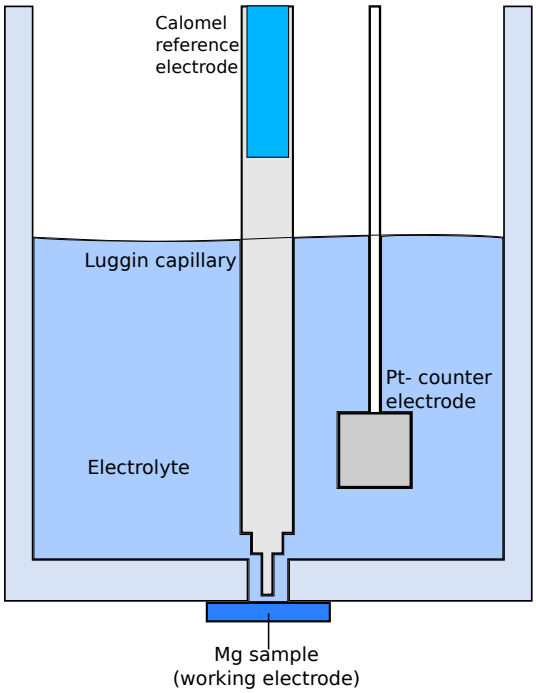

Figure 3.2 *Electrochemical cell setup*

3.2.1 Corrosion testing

Corrosion tests have been performed as voltammetrical measurements in the electrochemical cell setup to determine the corrosion protection capabilities of the coatings. The test parameters have been the same for all measurements. First the OCP was measured for $1800s$ and afterwards a pitting test performed. This test is a voltammetrical measurement and is stopped when a certain current I_{thres} is reached. The following parameters have been used in the experiments:

Table 3.3 *Parameters for corrosion test*

Parameter	Value
I_{thres}	$500\mu A$
U_{ini}	$-100mV$
SR	$1\frac{mV}{s}$
A_{WE}	$0.78525\ cm^2$
$M_{atom_{WE}}$	24.305
Valenz	2
ρ_{Mg}	$1.738\ \frac{g}{cm^3}$

With I_{thres} is the threshold current, U_{ini} is the initial potential in reference to the OCP, SR is the scan rate, A_{WE} is the area of the working electrode, $M_{atom_{WE}}$ is

the atom mass of the material of the working electrode and ρ_{Mg} is the density of magnesium.

3.3 Electro Microscopy

In this work most of the analysis was done with a SEM model XL40 from Philips with an EDAX CDU Leap detector. The microscope was used for EDX element analysis, topographical and element contrast images. The cleaned samples after heat treatment were glued with graphite pads on the specimen holder and did not need further preparations. To analyse the powders small amounts were placed on graphite pads and pressed on with a spatula. All samples were examined in a vacuum of $p < 5 \cdot 10^{-5} mbar$.

Cross-section polishes have been made for analysing diffusion layer more detailed. The polishes have been prepared by the metallography with a special vacuum embedding technique. The used resin was not conductive and the samples were metallised with graphite prior to analysis.

Elemental maps and line scan measurements have been performed in a JXA-8100 microprobe. This were the only measurements not taken by me, due to the complexity of the machine the responsible operator performed them.

4. RESULTS

4.1 Characterisation of slurry powder

The particle shape and size of the aluminium and zinc powder was determined with the SEM. Figure 4.1 shows the aluminium and zinc particles at different magnifications. Most of the aluminium particles have a spherical shape and the size distribution ranges from $140\mu m$ in figure 4.1(a) down to $5\mu m$ in figure 4.1(b) and less. The zinc particles have an elongated, piece like shape and range from tiny piece of about $10\mu m$ up to large hunks of $100\mu m$ and more.

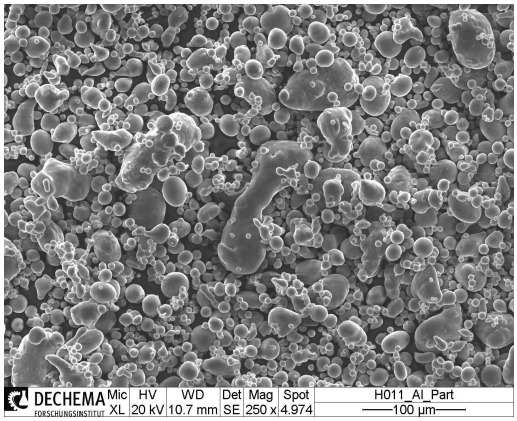

(a) Al-particle 250x magnification

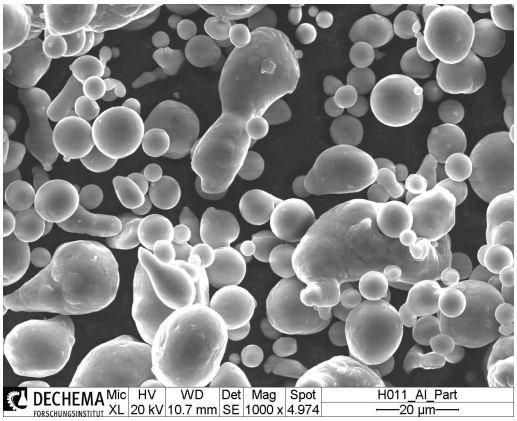

(b) Al-particle 1000x magnification

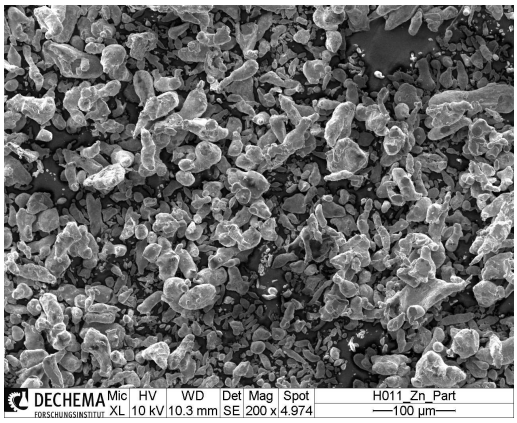

(c) Zn-particle 200x magnification

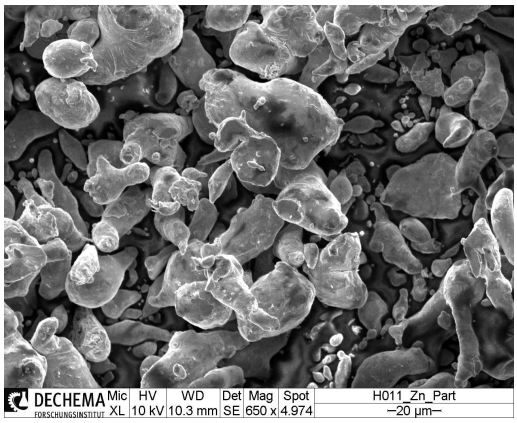

(d) Zn-particle 650x magnification

Figure 4.1 *SE-pictures of the used Al- and Zn-powders*

4.2 Characterisation of coatings

4.2.1 AZ31

Al-coating

As with all experiments of this work, the diffusion treatment has been carried out in an $Ar/5\%H_2$ atmosphere. Magnesium is a very reactive metal and reacts with even smallest amount of oxygen. Argon was chosen because of being inert and H_2 to reduce oxygen residuals or the oxide layer on magnesium. Experiments at temperatures of 450ï¿½C for 2h and 1h were performed. Additionally, an experiment at 420ï¿½C for 1h was performed. No experiment could confirm any kind of diffusion into the bulk. Figure 4.2 shows the aluminium particles from the powder and the underlying sample. As it can be seen in the element map for aluminium no diffusion into the bulk material and no interaction with the surrounding occurred. The line scan in figure 4.2(c) shows an enrichment of oxygen at the interface between resin and magnesium.

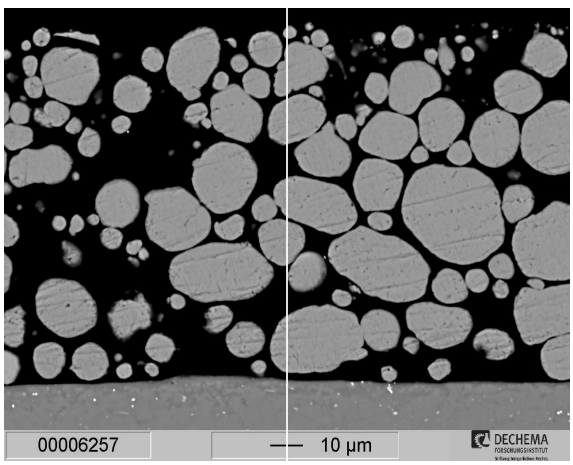

(a) BSE-image

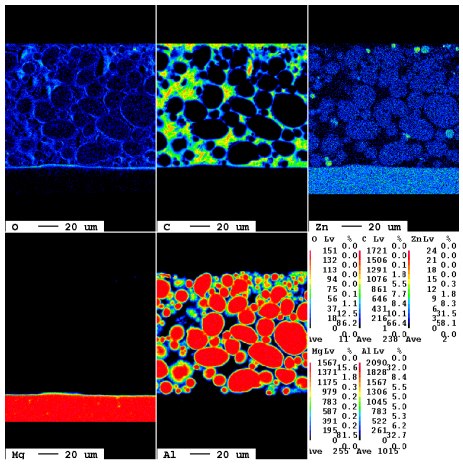

(b) Element map

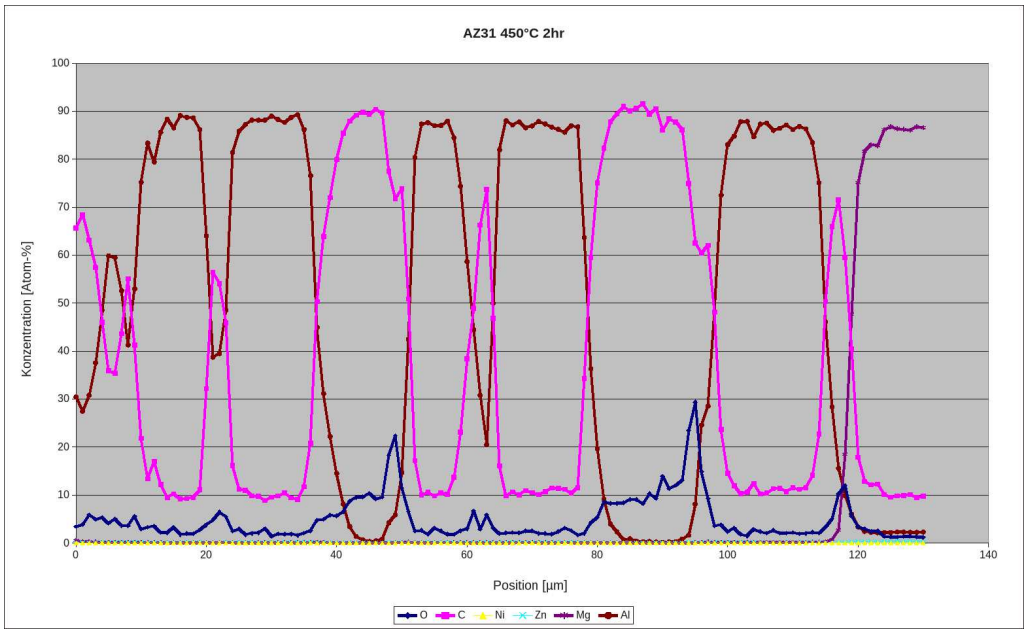

(c) Line scan along white line in (a)

Figure 4.2 *AZ31 heated at 450ï¿½C with Al-slurry for 2 hours*

Magnesium is a very reactive metal and forms oxides at very low partial oxygen pressure. The sample preparation method took the nature of magnesium as much into account as possible, but an oxidation of the surface is always present. Additionally, the residual oxygen in the process gas might have caused an additional oxidation of the sample. Nevertheless, Aluminium and carbon are also present in this particular area and, hence, there is no evidence of MgO formation. When comparing the aluminium particle in the layer with the original powder (see figure 4.1(a)), the coating layer seemed to be formed of agglomerated powder particles. The experiment at 420ï¿½C lead to the same result that the aluminium did not diffuse into the magnesium.

Zn-coating

The experiments with pure zinc slurry gave more favourable results than the aluminium experiments. Figure 4.3(a) shows the AZ31 sample after heat treatment at 450ï¿½C for 2h. The surface prior to the heating had a metallic shine, but had a dark/black colour with white spots afterwards. When wiping the surface with a paper towel black dust could be removed, but the sample not cleaned from it. Figure 4.3(a) shows a typical SEM micrograph of the surface. The surface is covered with a tight particle layer and under the SEM a differentiation between the white spots and the black coating is not possible.

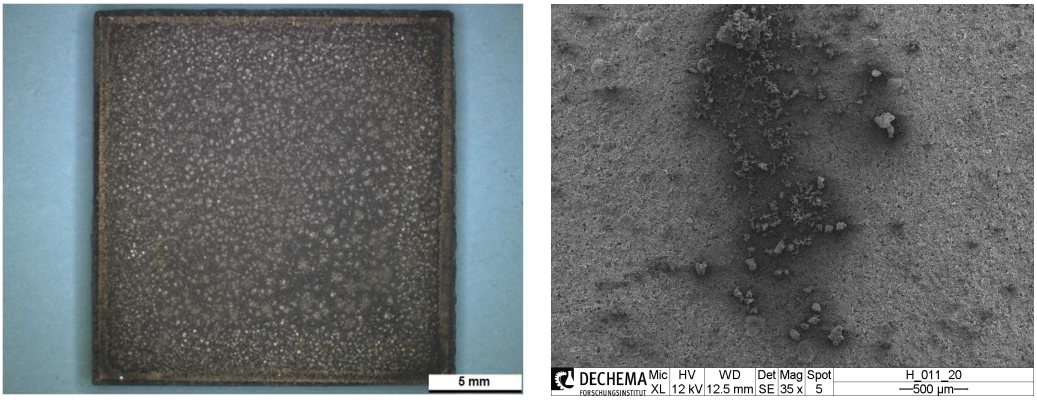

(a) Micrograph after heat treatment (b) SEM Micrograph after heat treatment

Figure 4.3 *Overview of Zn-coated sample at 450ï¿½C for 2h*

At a magnification of 1200x the single particles became visible as seen in figure 4.4. The particles should be composed of zinc and might have agglomerated as the aluminium particles. Investigations at 1500x magnification showed a different picture. The SE micrograph and, much better, BSE micrograph show a two phase nature of the particles. Some exhibit a coarse phase structure, whereas others show a very fine, barely visible phase structure. An EDX analysis of the particles shows that the particles with a fine phase distribution are composed of 69.1 $at\%\ Mg$, 21.3 $at\%\ Zn$, 8.3 $at\%\ O$ and 1.4 $at\%\ Al$.

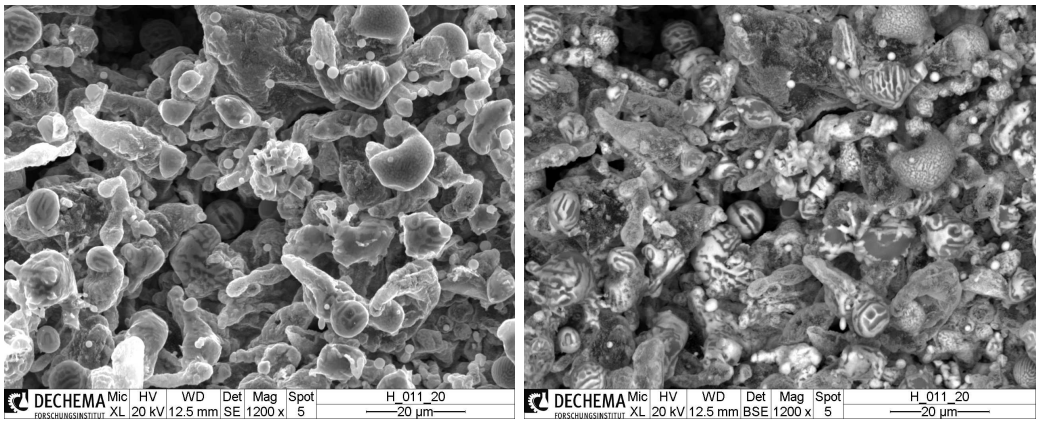

(a) SE micrograph (b) BSE micrograph

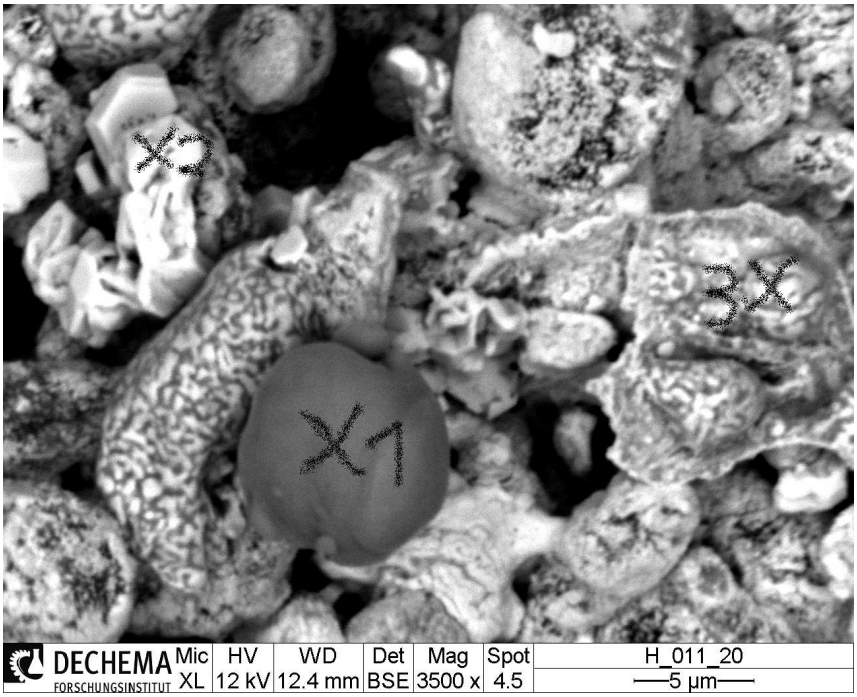

(c) Spots of EDX analysis

Figure 4.4 *Particles with different phases at 1200x magnification*

Later, to be able to perform corrosion measurements, the sample was cleaned with a toothbrush in VE water and is depict in figure 4.5. The cleaning process removed the complete particle layer and revealed a metallic layer on the sample surface. The layer has the appearance of a contracted skin and seems to have been formed from solidified liquid metal.

Figure 4.5 *Sample after thorough cleaning*

Figure 4.6(a) shows a BSE-image of cross-section polish and figure 4.6(b) the corresponding element mapping of oxygen, carbon, zinc, magnesium and aluminium. A white diffusion layer, which reaches up to several hundred μm deep, has formed. The element analysis in Fig. 4.6(b) suggests the formation of an Mg-Zn eutectic made up of single grains some with a coarse structure, others with a very fine structure. The composition was analysed with EDX and shows small deviations between fine and coarse phase structures in the magnesium and zinc content (see table 4.1).

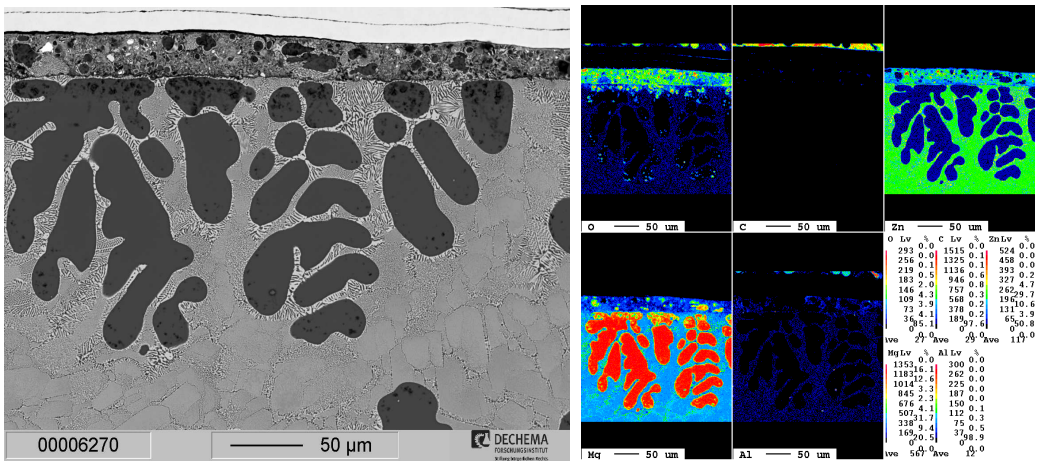

(a) BSE-image (b) Element map

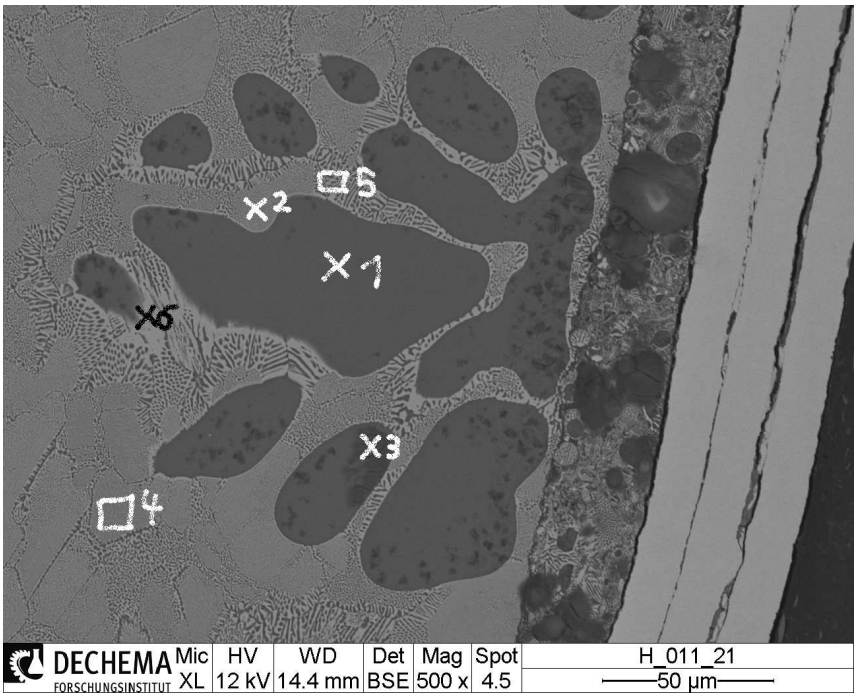

(c) Spots of EDX analysis

Figure 4.6 *AZ31 heated at 450ï¿½C with Zn-slurry for 2 hours*

	Fine structure	Coarse structure
Mg	69.7%	74.12%
Zn	28.1%	23.96%
Al	2.2%	1.9%

Table 4.1 *Elemental composition of the white phases in figure 4.6(a)*

Another main feature are large grey dendrites growing from the surface into the

diffusion layer. The element mapping in figure 4.6(b) shows a composition of magnesium with slight amounts of other elements. EDX measurements on the dendrites show a composition of $96,5\% Mg$ and $3,5\% Zn$ and small black spots near the sample surface and in the bulk. In some parts of the sample, these spots seem to effectively stop the diffusion of zinc (cf. Fig. 4.7). EDX analysis shows an enrichment of oxygen and maybe carbon. The element analysis in figure 4.6(b) verifies only an enrichment of oxygen.

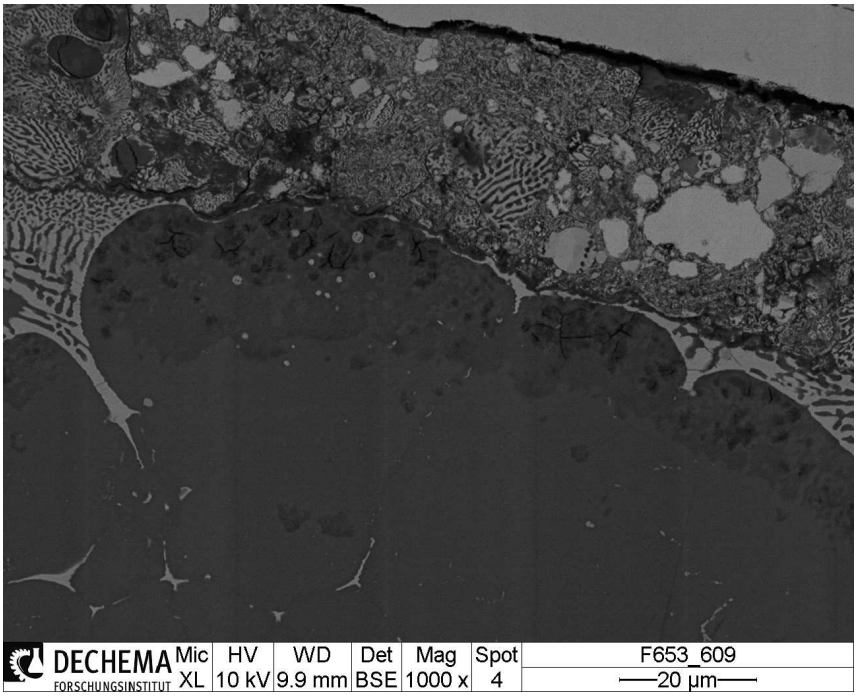

Figure 4.7 *Area of the sample in which MgO stopped the diffusion process*

Treatments at 420ï¿½C and 380ï¿½C show no indications of diffusion under WDX or EDX analysis. The sample heated at 420ï¿½C does not show any form of diffusion and the remaining powder on top of the sample could easily be removed. Neither the element analysis in figure 4.8 nor careful examination in the SEM could reveal any kind of oxide layer on the surface.

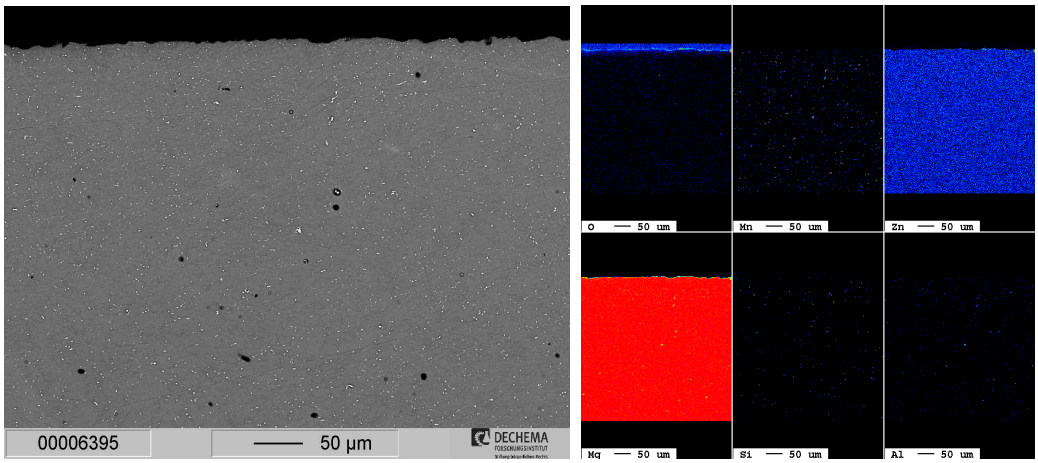

(a) BSE image (b) Element analysis

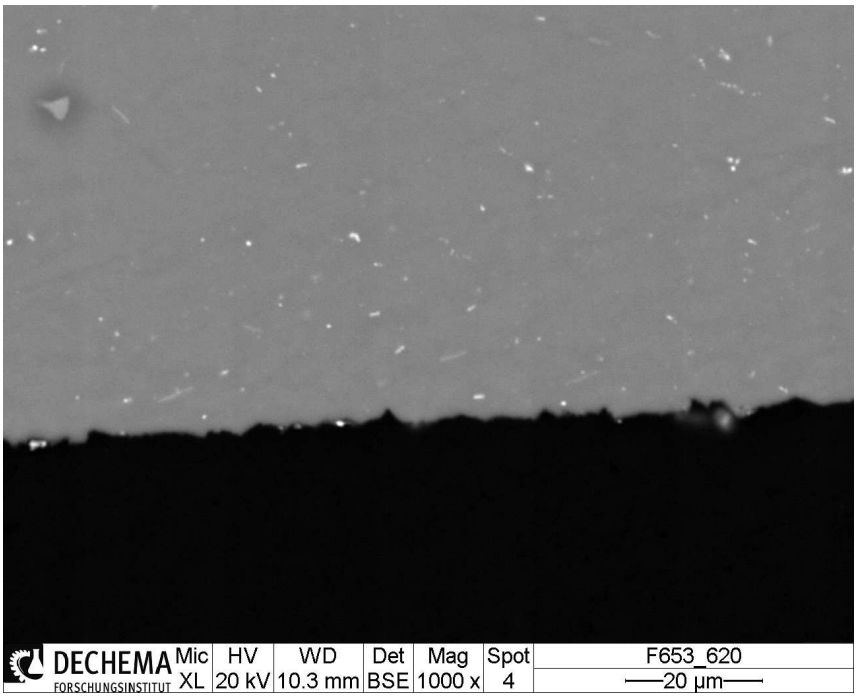

(c) SEM BSE image

Figure 4.8 *AZ31 heated at 420ï¿½C with Zn-slurry*

In general the results can be summarised that the diffusion of zinc into AZ31 was possible at a temperature of 450ï¿½C. At lower temperatures the diffusion did not occur.

Al-Zn coating

Experiments with aluminium-zinc slurry have been conducted at temperature of 450ï¿½C, 420ï¿½C and 380ï¿½C. Each heat treatment followed the protocol of reach-

ing the targeted temperature as fast as possible with low overshoot temperature and was carried out in an $Ar + 5\%H_2$ atmosphere.

The first experiment was a two hour heat treatment at 450ï¿½C as proof of principle. The slurry painted on the samples had a light gray colour and a mass of $0.1169g$. The solvent vaporised and left a light gray powder behind. Figure 4.9 shows the sample after heat treatment and SEM micrographs of the sample surface. The appearance of all following samples was similar to this one.

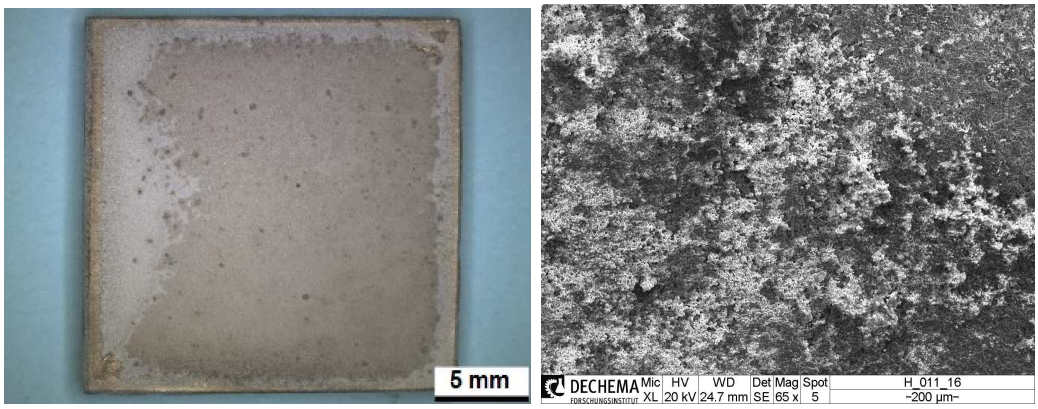

(a) Sample after heat treatment

(b) SE picture of the surface

(c) SE picture of the surface

Figure 4.9 *AZ31 heated at 450ï¿½C for 2h with an Al-Zn slurry*

Figure 4.10(a) shows a detail of the corresponding cross-section polish containing the rest of the slurry on top of the sample, a diffusion layer and, at the bottom of the figure, the base material. The black colour in the BSE micrograph is the embedding material, a non-conductive resin. The diffusion layer consists of several phases, a magnesium and aluminium rich phase, a zinc rich phase and a magnesium rich phase as illustrated in figure 4.10(b). All of these phases are distributed in the sample and as particles on the surface resembling the aluminium particles used

to make the slurry. The aluminium-magnesium phase is widely distributed and matches the lighter phase in figure 4.10(a). It does not only contain magnesium and aluminium, but slight amounts of zinc and oxygen. A ternary phase of Al-Mg-Zn might have been formed. Next to the light gray phase are small amounts of a white phase mostly existing in the diffusion layer and in the form of particle shells in the coating layer. The element analysis shows that in this regions zinc and oxygen are enriched. Despite the enrichment of zinc, it is surprisingly scarce assuming that the slurry contained equal parts of aluminium and zinc.

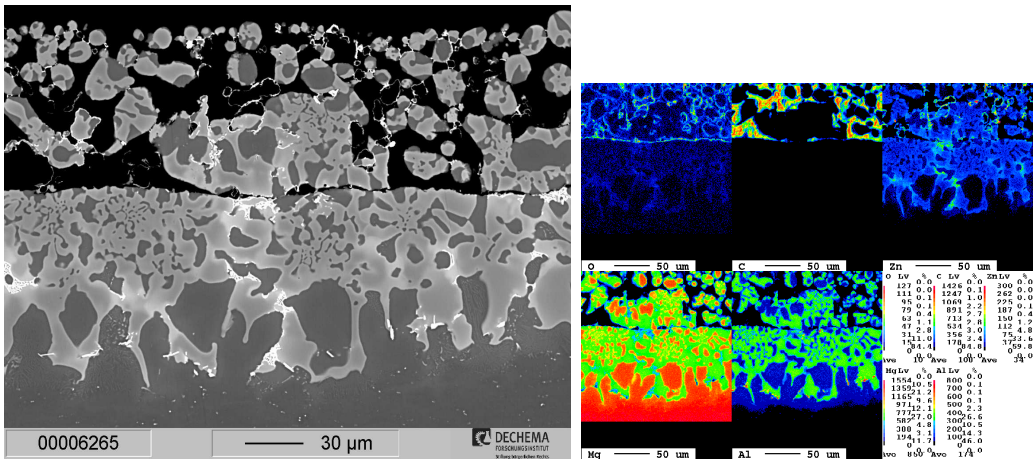

(a) BSE image (b) Element analysis

Figure 4.10 *AZ31 after heat treatment at 450ï¿½C for 2h with Al-Zn slurry*

The phases were determined by a line scan (see figure 4.11). The light gray phases consist of mainly magnesium with a large fraction of aluminium and minor content of zinc. The bright white phases could not be measured with enough precision, because the combination of spot size and minimum step width ($1\mu m$). Nevertheless, the zinc signal rises in these areas and leads to the assumption that zinc is enriched there.

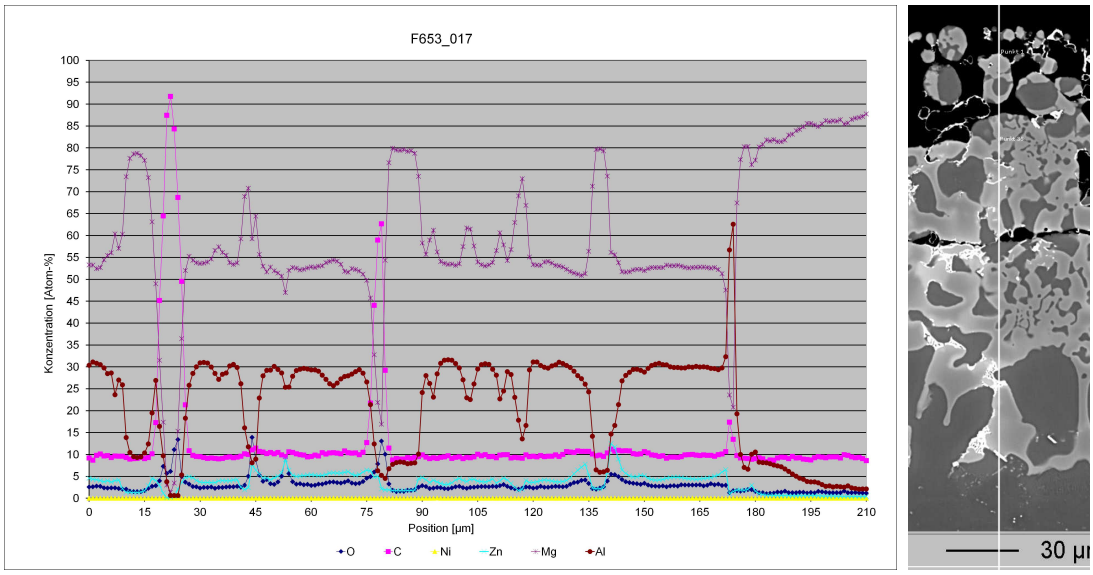

(a) Element linescan (b) Linescan

Figure 4.11 *Element analysis of the different phases of the diffusion layer along the white line in the right figure.*

The bulk material is made of magnesium, but the aluminium content seems to be higher in the dark, base material like areas than in the middle of the sample. The line scan in figure 4.11(a) shows a declining aluminium content until $200\mu m$.

	Mg [%]	Al [%]	Zn [%]
Light grey phase	54%	30%	5%
Dark grey phase	80%	8%	3%
White phase	$\approx 55\%$	$\approx 15\%$	$\approx 12\%$

Table 4.2 *Composition of phases in figure 4.10*

Heat treatment at 450ï¿½C for 1h

At a temperature of 450ï¿½C and a treatment duration of 1h the picture is vastly different. Figure 4.12(a) shows the diffusion layer of the 1h heat treatment. The diffusion layer is about $285\mu m$ thick and has a much finer structure than the sample with a 2h duration. Other features are the big white precipitations similar to the previous sample. An element map (figure 4.12(b)) reveals that they consist mainly of zinc with parts of magnesium and aluminium. The particles covering the sample exhibit a three layer structure with aluminium particle on top, particles made of an Al-Mg phase in the middle and particles with the same phases as the diffusion layer on the sample surface as displayed in figure 4.13.

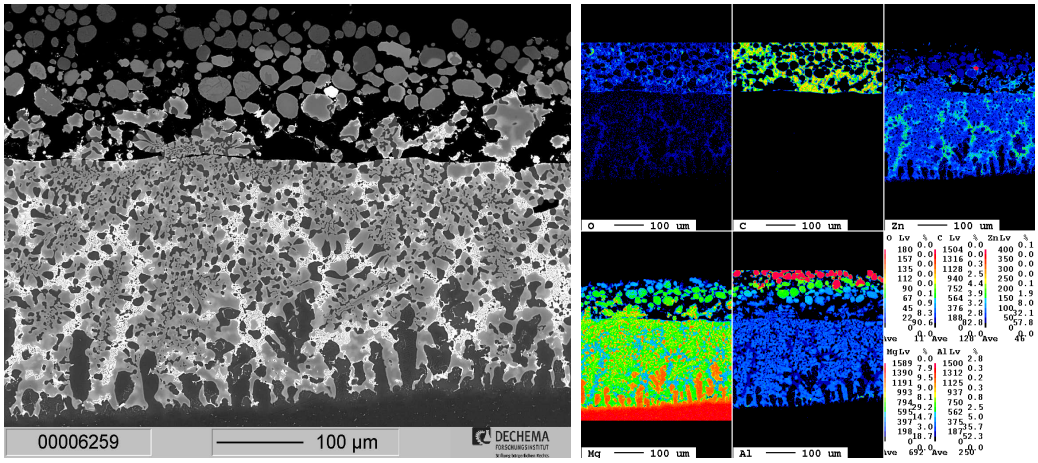

(a) BSE image (b) Element analysis

Figure 4.12 *AZ31 after heat treatment at 450ï¿½C for 1h with Al-Zn slurry*

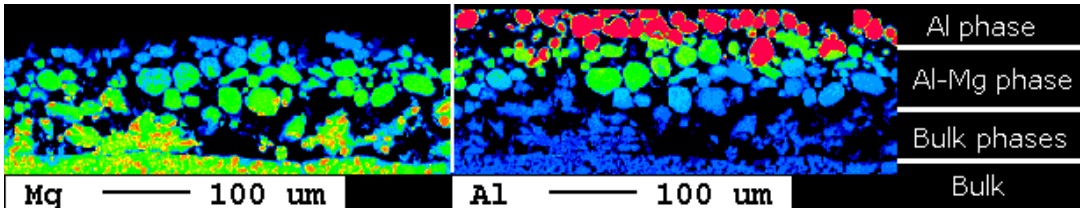

Figure 4.13 *Different phases in the particle layer*

At a temperature of 420ï¿½C the picture is completely opposite the heating at 450ï¿½C. Figure 4.14 shows the SE and BSE image of a cross-section polish. No diffusion at all is visible and most remarkably is the shape of the Al and Zn particles. The big Zn particles (white particles in the picture) do not seem to have agglomerated or even been molten. The melting temperature of zinc is with 419.53ï¿½C just at the heating temperature, so a partial melting would be expected. Additionally, the oven tends to overshoot in the temperature, thus the likelihood of reaching the melting temperature is certain.

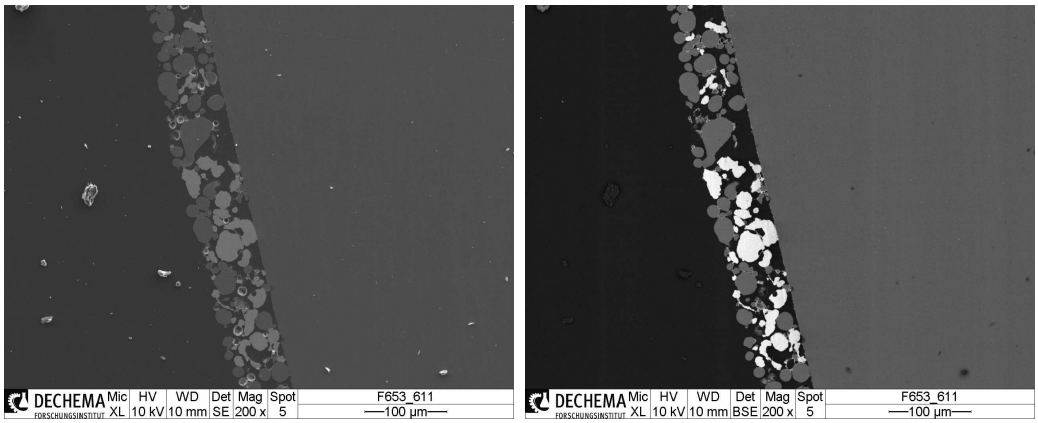

(a) SE Image (b) BSE Image

Figure 4.14 *AZ31 heat treated at 420ï¿½C with Al-Zn slurry*

Based on these results, the missing of particle agglomeration for zinc and aluminium, and metallic shine of the sample after cleaning, no further analysis had been done on the sample.

Similar to the previous results are these for heating at 380ï¿½C. Microprobe analysis (see figure 4.15) shows no diffusion of neither zinc nor aluminium into the material. The only feature is a band of oxygen enrichment in about 200 μm depth.

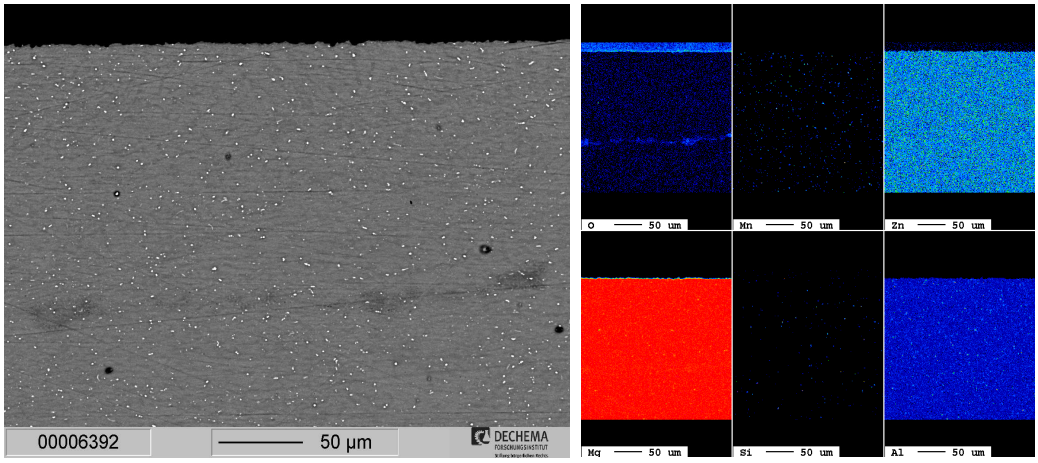

(a) BSE image (b) Element analysis

Figure 4.15 *AZ31 after heat treatment at 380ï¿½C for 1h with Al-Zn slurry*

4.2.2 AZ91

Al-coating

The Al coating experiments on AZ91 showed similar results as AZ31. Figure 4.16(a) shows a cross-section polish from a sample treated at 450ï¿½C for 1 h. It can be seen that no intermetallics have been formed nor aluminium segregated and the β phase of AZ91 is not present. Figure 4.16(b) shows a element analysis of the sample and supports that no intermetallics have been formed. Additionally, a uniform aluminium distribution can be observed with an average aluminium contend of $8\% Al$. Thus, no diffusion of aluminium occurred at a temperature of 450ï¿½C.

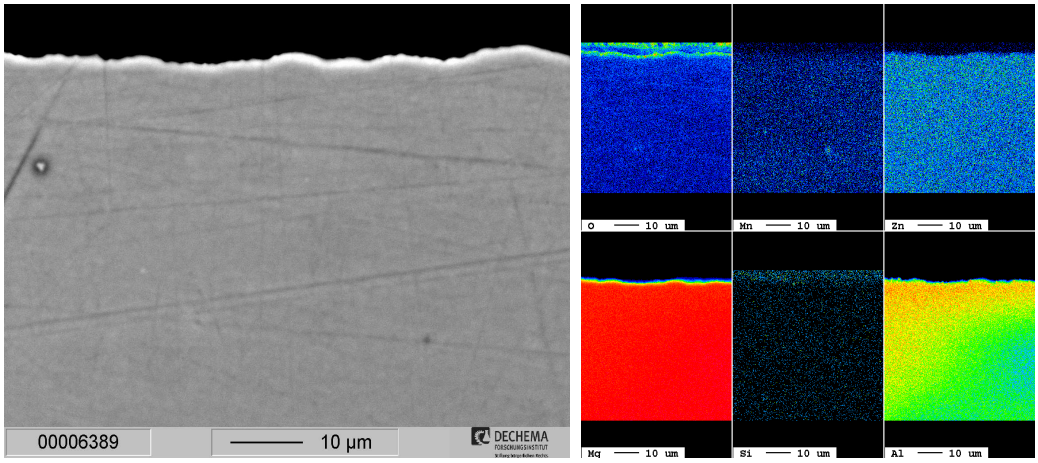

(a) BSE image (b) Element maps

Figure 4.16 *AZ91 heated at 450ï¿½C with Al-slurry*

Figure 4.17 shows a SEM image of the sample treated at 420ï¿½C with remaining aluminium powder on the sample. The aluminium particles do not exhibit any changes compared with the original particles (see figure 4.1(a)). The surface on the other hand changed, as the scratch marks from grinding are only slightly present. Figure 4.16(b) shows an enrichment of oxygen at the sample surface.

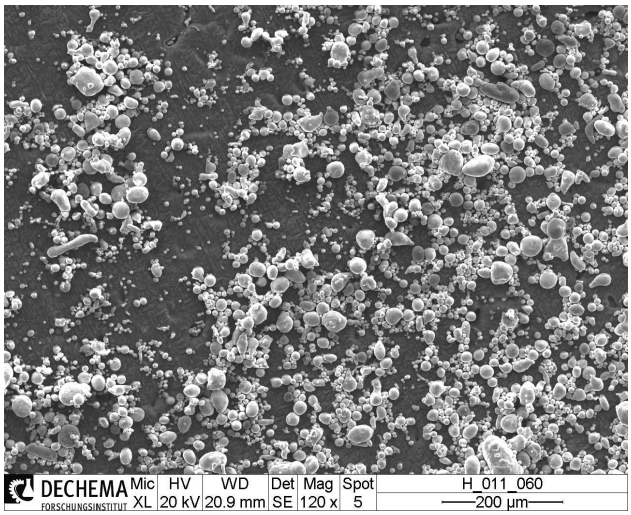

Figure 4.17 *SEM micrograph of AZ91 Al slurry coated at 420ï¿½C*

Zn-coating

Experiments with a zinc rich slurry have been performed at 450ï¿½C, 420ï¿½C and 380ï¿½C each with a treatment duration of 1 hour. The results are similar to these of AZ31 and show in general a diffusion of zinc into the substrate. Figure 4.18 shows the microprobe analysis of a sample heated at 450ï¿½C. Three different phases have been formed a white zinc rich phase, an eutectic phase of zinc and magnesium and a grey aluminium rich phase. Line scans taken from these samples show a very high carbon content ($\approx 30at\%$) in the magnesium phases and render them unusable. Therefore, they are not included in this work.

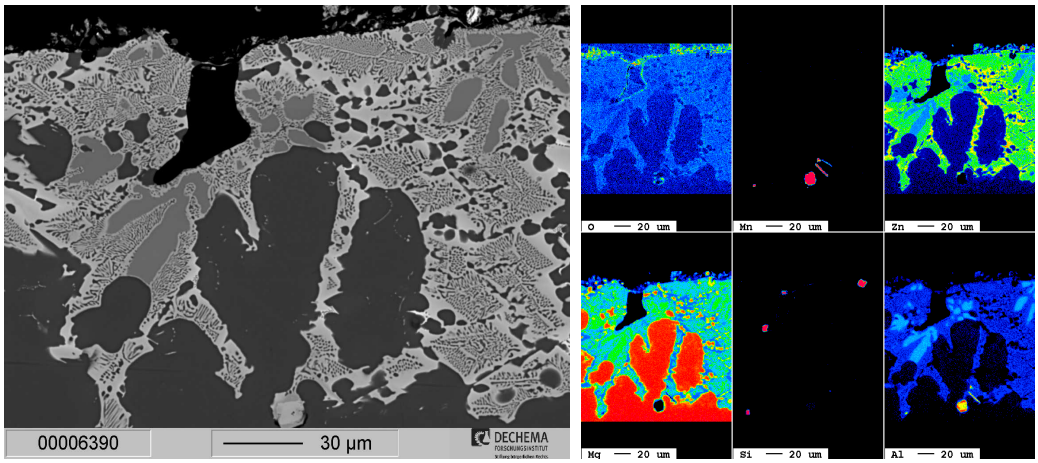

(a) BSE Image (b) Element analysis

Figure 4.18 *Cross-section polish of AZ91 treated at 450ï¿½C with Zn-Slurry*

Another similarity to the AZ31 samples is the formation of dendrites made out of the base material. Not only zinc and aluminium, but also manganese and silicium precipitations are visible. Manganese is a common alloy element (see chapter 2.1.1) and is used together with aluminium. It is always present in magnesium alloys to reduce the iron content to an acceptable amount. The heat treatment might have caused segregations in this case.

As the experiments with AZ31 showed, no diffusion into the material occurred at a temperature of 420ï¿½C or below. The sample looks like a typical AZ91 sample, with a two phase structure as seen in figure 4.19(a). Noticeable are a few manganese precipitations and a band rich of oxygen in a depth of about $700\frac{1}{2}m$.

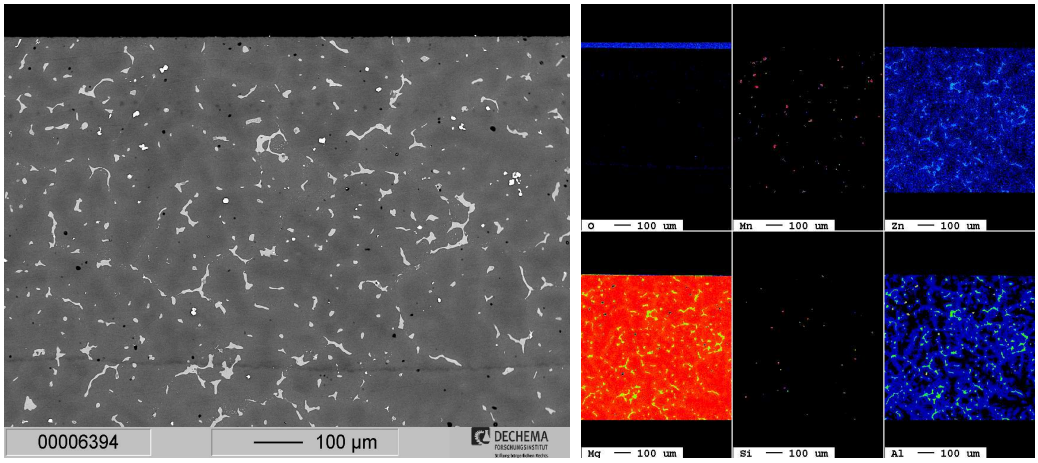

(a) BSE image (b) Element maps

Figure 4.19 *AZ91 heated at 420ï¿½C with Zn slurry*

Al-Zn coating

At 450ï¿½C with a treatment time of 1h a similar picture can be seen as for the AZ31. A zinc rich phase formed near the surface with Mg rich dendrites. The slurry particles show the same phase structure and also seem to have agglomerated. Figure 4.20(a) shows a BSE picture of the diffusion layer. The white areas are mainly manganese precipitations according to the elemental map in figure 4.20(b). The line scans taken from these samples show a very high carbon content ($\approx 30at\%$) in the magnesium phases and render them unusable. Therefore, they are not included in the this work.

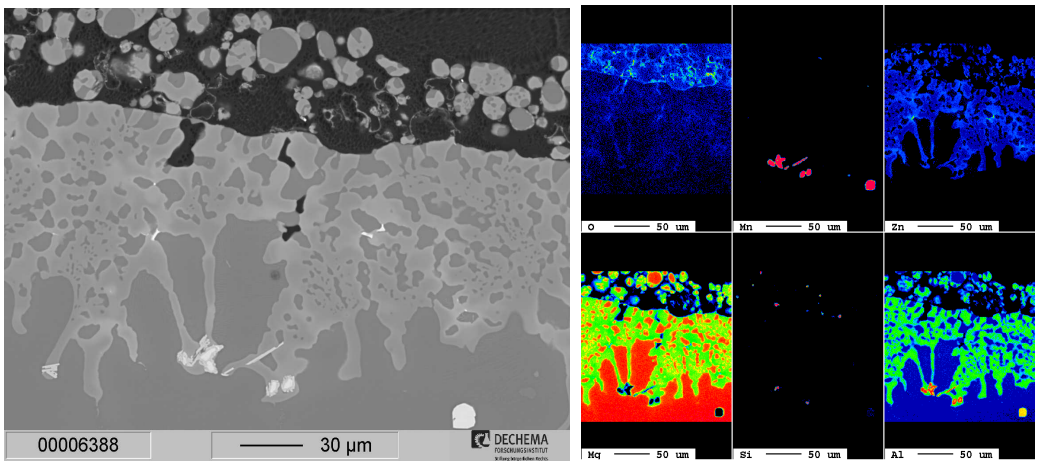

(a) BSE-Image (b) Element analysis

Figure 4.20 *Diffusion layer on AZ91 after treatment with a Al-Zn slurry at 450ï¿½C*

In further experiments the temperature was lowered to 420ï¿½C with complete different results than before. Figure 4.21 displays a BSE image of a cross-section polish from the slurry-sample interface together with the respective element analysis. In contrast to figure 4.20 no diffusion is visible neither in the BSE image nor in the element analysis. The typical AZ91 contains α-Mg and β-Mg phases, with the light grey phases in figure 4.21(a) being β-Mg. Next to this two phases, few Mn precipitations are visible. Mn is a common alloying element and "iron trap" as written in section 2.1.1.

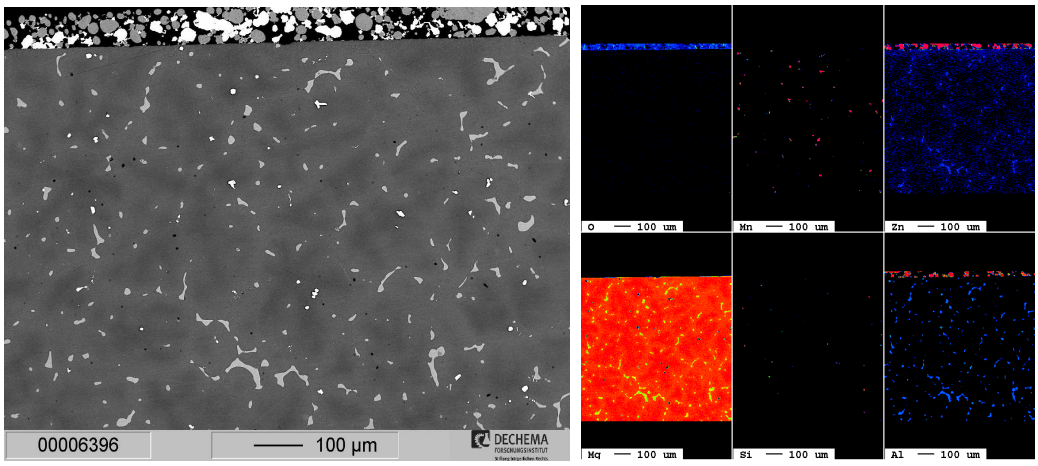

(a) BSE-Image (b) Element analysis

Figure 4.21 *Cross-polish micrographs of AZ91 heated at 420ï¿½C with Al-Zn slurry*

Another experiment at 380ï¿½C showed no sign of a diffusion of neither zinc nor aluminium into the magnesium.

4.3 EC-characterisation of coatings

4.3.1 AZ31

As first corrosion test the plain material was tested to establish a baseline for further testing. The reference measurements on AZ31 only grinded with 1000er SiC paper is displayed in figure 4.22.

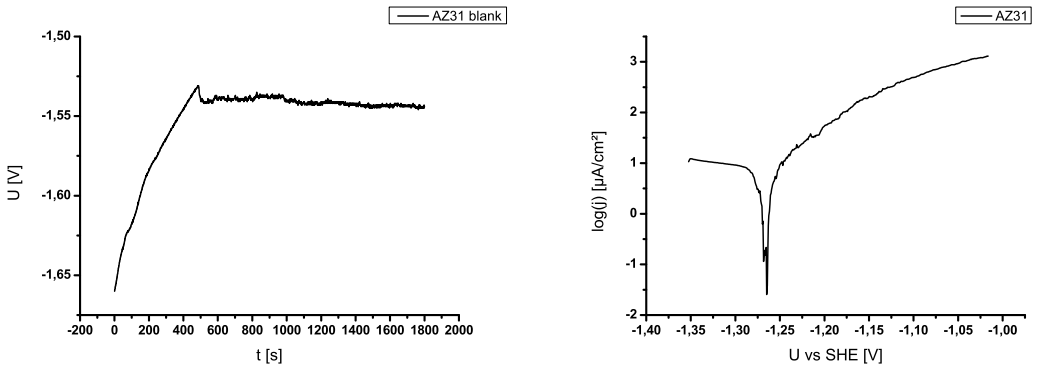

(a) OCP measurement (b) Pitting test

Figure 4.22 *OCP and pitting results from grinded AZ31*

After 1800s immersion in $0.05 MNaCl$ solution the OCP stabilised at a value of $1.55 Vvs.SHE$. The pitting test shows a distinct anodic behaviour with steadily increasing current density and a very small cathodic part. The corrosion current density is $1.55 \cdot 10^{-1} \frac{\mu A}{cm^2}$ at a potential of $E_{corr} = -1.263\ V\ vs.\ SHE$ In the following are the corrosion test results for the Zn and Al-Zn coating. The samples with a pure Al slurry were not tested, due to the lack of a diffusion layer.

Zn-coating

The zinc coating shows in general two different corrosion profiles, as it can be expected from the coatings results. Figure 4.23(a) shows the OCPs from the zinc experiments. The two coatings at 450ï¿½C show an E_{corr} about +100mV more anodic than the reference. Similar results come from the corrosion test depict in figure 4.23(b). The shape of the corrosion current for the blank, 420ï¿½C and 380ï¿½C are indication for pitting followed by a stable corrosion.

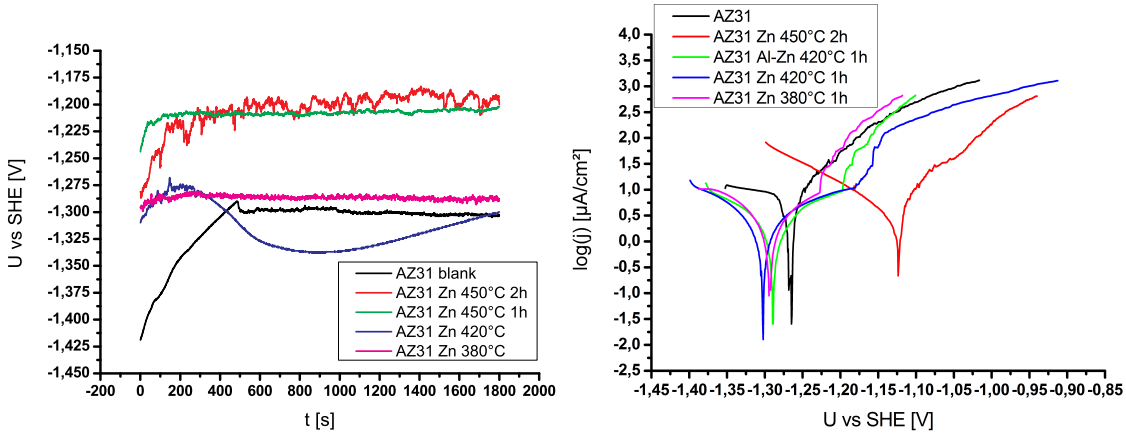

(a) OCP measurements (b) Potentio dynamic polarisation curve

Figure 4.23 *Corrosion measurements of AZ31 Zn coatings*

Al-Zn coating

Figure 4.24 shows the OCP and pitting measurements for the AZ31 coated with AlZn at various temperatures. The results are similar to the previous ones and only the coating at 450ï¿½C shows a significant increase in the OCP of about +160mV. The potentiodynamic polarisation curve for 450ï¿½C shows a very long cathodic branch. Song et al. [4] described occluding of cracks and pits by hydrogen bubbles during corrosion and formation of local anodes and cathodes inside these isolated cracks. Furthermore, it is not possible to measure the corrosion inside the isolated cracks. Considering the experimentation setup, it seems likely that the anodic sides on the sample have been isolated by hydrogen bubbles, so that only the cathodic reaction could be observed.

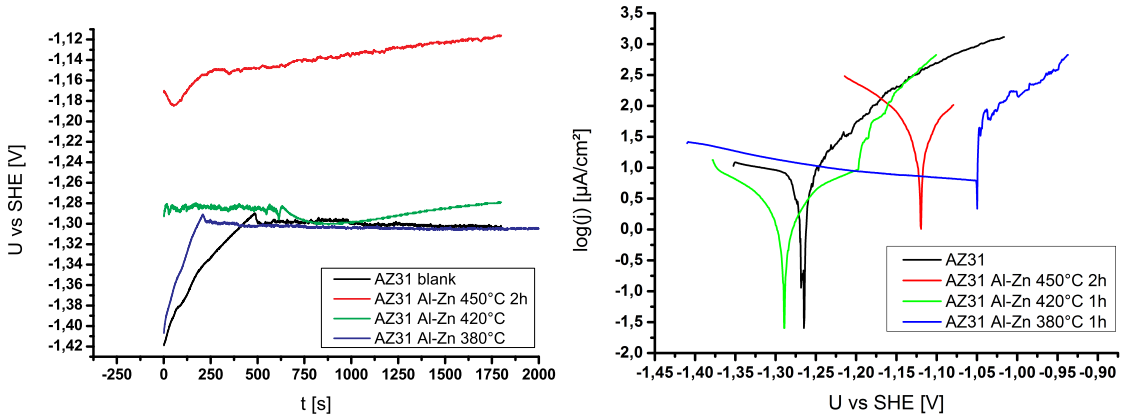

(a) OCP measurements (b) Potentio dynamic polarisation curve

Figure 4.24 *Corrosion measurements of AZ31 AlZn coatings*

4.3.2 AZ91

Zn-coating

The corrosion measurements on AZ91 have similar results to those of AZ31. All samples have an OCP similar to that of the reference, except the 450ï¿½C sample as displayed in figure 4.25(a). The potentio dynamic polarisation results reflect the OCP measurements and only the 450ï¿½C sample shows an improved corrosion resistance.

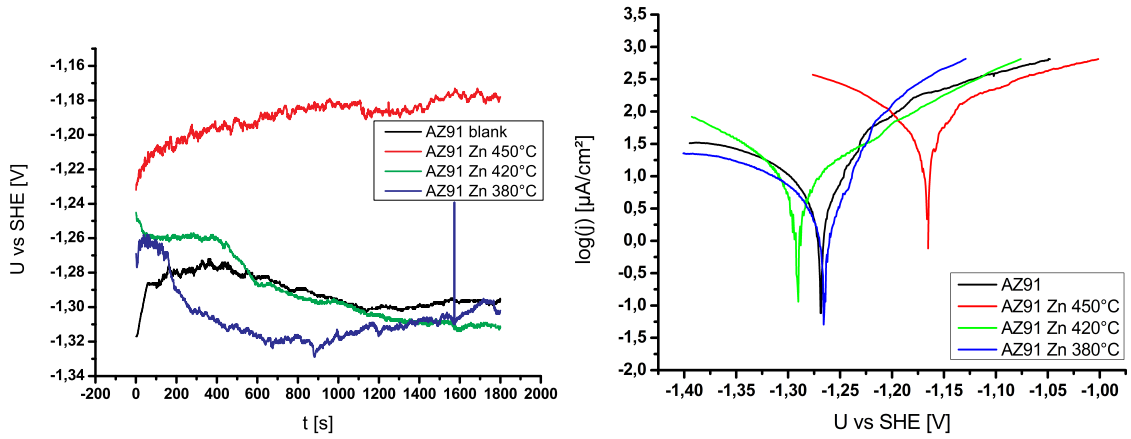

(a) OCP measurements (b) Potentio dynamic polarisation curve

Figure 4.25 *Corrosion measurements of AZ91 Zn coatings*

Al-Zn coating

Similar to the Zn coating, only the sample heated at 450ï¿½C showed a changed OCP and E_{corr} during potentio dynamic polarisation measurements.

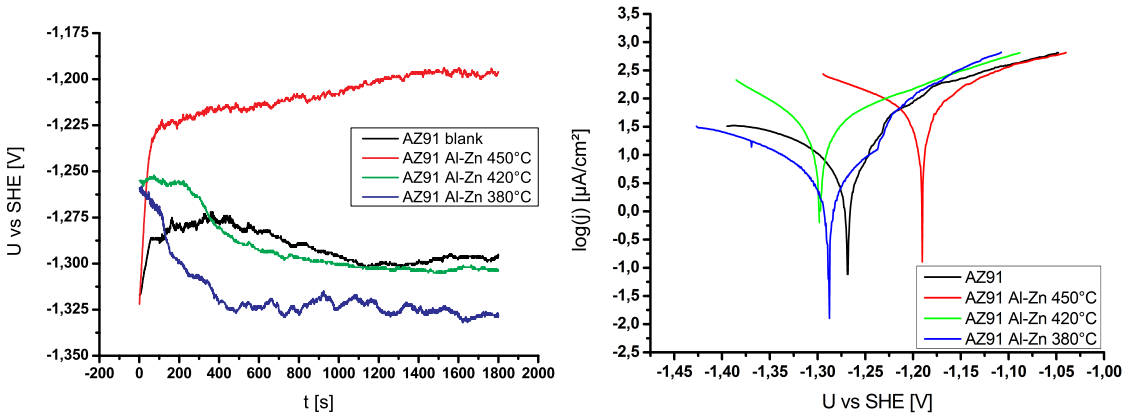

(a) OCP measurements (b) Potentio dynamic polarisation curve

Figure 4.26 *Corrosion measurements of AZ91 AlZn coatings*

5. DISCUSSION

The experiments of this work gave a few interesting results and the most significant is the formation of a diffusion layer only at a temperature of 450ï¿½C regardless the slurry or basic material, except that no diffusion layer could be produced using a pure Al-slurry. Several effects might have hindered its diffusion and promoted Zn and Zn-Al slurries. Hirmke et al. [29] studied packed powder diffusion with Al-Zn on AZ91E and concluded that the addition of Zn to the Al powder significantly promotes the formation of intermetallic layers. In their paper they report of diffusion layers as thick as $600\mu m$ for T as low as 350ï¿½C. Nevertheless, their procedure requires treatment times of up to 18h. The results show that the addition of Zn in the slurry powder promotes the diffusion of Al and the formation of ternary Mg-Al-Zn phases. All of the phases are very Mg rich and their composition is summarised in table 5.1

Phase	Material	T [ï¿½C]	t [hr]	Coating	Composition
Fine structure	AZ31	450	2	Zn	$Al_1Mg_{35}Zn_5$
Coarse structure	AZ31	450	2	Zn	$Al_2Mg_{91}Zn_{10}$
Light grey	AZ31	450	2	Al-Zn	$Al_{14}Mg_{28}Zn_1$
Dark grey	AZ31	450	2	Al-Zn	$Al_6Mg_{72}Zn_1$
White precipitations	AZ31	450	2	Al-Zn	$Al_6Mg_{25}Zn_2$

Table 5.1 *Formed phases in diffusion layers on AZ31*

In all the samples the diffusion coating contained areas of the crude basic material in the form of dendrites. EDX analysis showed that oxidic Mg particles segregated at the upper part of the dendrites. Additionally, the samples at 420ï¿½C, with no diffusion layer, contain a thin oxide layer on the surface. The corrosion measurements on these samples show pitting characteristics and the local breakdown of a protective film as common for magnesium [30]. The oxidic Mg particles seem to prevent diffusion effectively and should be the reason why no pure Al was observed. The difference in the Zn experiments can be explained by the liquefaction of Zn at a temperature of 420ï¿½C. In the 450ï¿½C experiments the Zn was liquid and caused a breakthrough through the protective surface layer. At lower temperatures the Zn did not melt totally and could not aid the oxide breaking process.

In the SEM micrographs it is visible that the slurry particles show a similar intermetallic phase structure as the diffusion layer. Hirmke et al [29] presented a schematic description of the diffusion dynamics during the PPDC process. It seems viable to assume a similar mechanism here, namely that the particles also diffuse into each other, into the magnesium and the magnesium into them. Zn will diffuse mainly into the Al-particles, since the solubility of Zn in Al is much higher ($\approx 64\%$ [29]) than Al in Zn ($\approx 2\%$ [29]). Thus when the Zn started to melt it got solved in the Al particles and the magnesium substrate. However, Czerwinski [31] investigated the oxidation behaviour of AZ91D at high temperatures and reported sublimation of magnesium. The sublimation was guided by the oxidation process and Al content. High Al contents of 10% seem to increase the rate-constant at 673K by over two order of magnitude. In general it was assumed that an increased oxidation rate was the major driver for magnesium sublimation. Furthermore, Czerwinski pointed out a similar oxidation acceleration effect for zinc. The slurries which produced diffusion layers had all a high zinc content ($50wt.\%$ & $25wt.\%$) and half of them additionally a high aluminium content ($25wt.\%$). It seems likely that the zinc and aluminium together supported the formation of semi-solid magnesium, which then sublimated and interacted with the powder particles on top of the sample.

The EC measurements showed that the diffusion coatings increase the corrosion resistance of AZ31 and AZ91. The shape of the potentio dynamic polarisation curves is typical for magnesium and its alloys [3], [4], [21], [22], [29], [32]–[34]. From this it follows, that the specimen corroded locally plus figure 5.1 shows very localised black spots on the surface.

Figure 5.1 *AZ31 after corrosion test*

The potentio dynamic polarisation curves seem to follow the course of a typical tafel plot. King et al. [21] compared several techniques regarding the preciseness of the measured corrosion rate and reported that Tafel extrapolation gives too small values. Tafel extrapolation is based on the assumption that the surface corrodes uniformly and not locally as with magnesium [16]. The corrosion mechanism of all samples is the same that a thin partially protective layer (not the diffusion layer) exists on the surface and leads to the phenomena of pitting after local breakdown. The higher E_{corr} of the successfully coated samples results from the enrichment of zinc in the diffusion layer. Joensson [35] describes in his PhD thesis that zinc does not increase the corrosion protection of magnesium, but introduces an anodic shift of E_{corr}.

6. CONCLUSION

1. The diffusion process can easily be hindered by the natural surface oxide layer of magnesium. At high temperatures (>450ï¿½C) the protection of the layer is not enough to stop the diffusion, but at lower temperatures (<= 420ï¿½C) all diffusion is blocked.

2. Zn aids the diffusion of Al by lowering the melting point and promotes the formation of ternary Mg-Al-Zn phases. Molten zinc on the surface can break the protection of the surface oxide layer and enable diffusion into the magnesium.

3. The diffusion process is guided by a mass exchange between the Zn particles, the Al particles and the Mg substrate. All of them diffuse into each other and change their physical properties respectively. Furthermore the addition of zinc causes the aluminium and magnesium to melt at lower temperatures and thus supported the evaporation of semi-solid magnesium.

4. Zinc as major part in the diffusion layer does not bring the hoped for corrosion protection. E_{corr} is increased due to the higher zinc content, which would reduce galvanic corrosion potential, but i_{corr} is not influenced by the zinc content.

7. OUTLOOK

The topic of corrosion protection through diffusion layer coating proved to be a challenging and interesting topic with a great potential to supply easy and cheap access to corrosion resistance improved magnesium. This work shall be seen as proof of principle and the basic layout for further research. Many variables play a role in the formation of good diffusion coatings and the most important, from my point of view, are:

Treatment time Influences the layer thickness, ability to break the surface oxide layer and economical efficiency of the process.

Surface oxide layer Critical parameter on the way to low temperature application and hinders diffusion of third metals effectively. In further research the introduction of an oxide breaker as known from packet powder diffusion might be helpful. Another option is the removal by pickling, e.g. with an aluminium pickle.

Gas atmosphere Oxygen seems to be a harmful element to the whole process and methods of reducing the residual oxygen level to an ϵ level (0%) seems worthwhile.

Slurry composition Different compositions yield different diffusion layers. Worthwhile implementing should be the design of different slurries according to the other parameters, such as treatment time and temperature.

Temperature Similar to treatment time, the temperature plays a major role in the whole process and an optimum between layer thickness, composition, time and temperature should be found. Nevertheless, from an economic standpoint the aim should be for lower temperatures.

Process Integration into existing industrial processes would not only reduce the costs, but can also benefit the overall environmental conditions.

BIBLIOGRAPHY

[1] B. Mordike and T Ebert, "Magnesium: Properties - applications - potential", *Materials Science and Engineering: A*, vol. 302, no. 1, pp. 37–45, 2001, ISSN: 0921-5093.

[2] S. Feliu, A. Pardo, M. Merino, A. Coy, F. Viejo, and R. Arrabal, "Correlation between the surface chemistry and the atmospheric corrosion of AZ31, AZ80 and AZ91D magnesium alloys", *Applied Surface Science*, vol. 255, no. 7, pp. 4102–4108, 2009, ISSN: 0169-4332.

[3] C. CAI, Z. Zhang, Z. ling Wei, J. feng Yang, and J. feng Li, "Electrochemical and corrosion behaviors of pure Mg in neutral 1.0% NaCl solution", *Transactions of Nonferrous Metals Society of China*, vol. 22, no. 4, pp. 970–976, 2012, ISSN: 1003-6326.

[4] A. Atrens, G.-L. Song, M. Liu, Z. Shi, F. Cao, and M. S. Dargusch, "Review of recent developments in the field of magnesium corrosion", *Advanced Engineering Materials*, n/a–n/a, 2015, ISSN: 1527-2648.

[5] "Elektron 21, Datasheet 455", Magnesium Elektron UK, 2006. [Online]. Available: `http://www.magnesium-elektron.com/data/downloads/DS455.PDF` (visited on 12/11/2014).

[6] H. Friedrich and B. Mordike, Eds., *Magnesium Technology*. Springer, 2006, ch. 3, ISBN: 3-540-20599-3.

[7] Y. Narukawa, K. Watanabe, K. Matsuda, T. Kawabata, and S. Ikeno, "Effect of Zn Contents on Microstructure in AZ-series magnesium alloys", *Advanced Materials Research*, vol. 409, pp. 358–361, 2011.

[8] M. Liu, P. J. Uggowitzer, A. Nagasekhar, P. Schmutz, M. Easton, G.-L. Song, and A. Atrens, "Calculated phase diagrams and the corrosion of die-cast mg-al alloys", *Corrosion Science*, vol. 51, no. 3, pp. 602 –619, 2009, ISSN: 0010-938X.

[9] H. Friedrich and B. Mordike, Eds., *Magnesium Technology*. Springer, 2006, ISBN: 3-540-20599-3.

[10] G. S. Cole, "Issues that influence magnesium's use in the automotive industry", *Materials Science Forum*, vol. 419-422, pp. 43–50, 2003.

[11] "Corrosion and oxide films", in, A. Bard and M. Stratmann, Eds., 4 vols., ser. Encyclopedia of Electrochemistry. Wiley-VCH, ch. 1, ISBN: 3-527-30396-0.

[12] T.-S. Shih, J.-B. Liu, and P.-S. Wei, "Oxide films on magnesium and magnesium alloys", *Material Chemistry and Physics*, vol. 52, no. 104, pp. 497–504, 2007, ISSN: 0254-0584.

[13] H. Friedrich and B. Mordike, Eds., *Magnesium Technology*. Springer, 2006, ch. 7, ISBN: 3-540-20599-3.

[14] C. Wagner and W. Traud, "Über die deutung von korrosionsvorgängen durch überlagerung von elektrochemischen teilvorgängen und über die potentialbildung an mischelektroden", *Zeitschrift für Elektrochemie und angewandte physikalische Chemie*, vol. 44, no. 7, pp. 391–402, 1938, ISSN: 0005-9021.

[15] "Corrosion and oxide films", in, A. Bard and M. Stratmann, Eds., 4 vols., ser. Encyclopedia of Electrochemistry. Wiley-VCH, ch. 5, ISBN: 3-527-30396-0.

[16] E. McCafferty, *Introduction to Corrosion science*. Springer New York, 2010.

[17] M. Liu, S. Zanna, H. Ardelean, I. Frateur, P. Schmutz, G. Song, A. Atrens, and P. Marcus, "A first quantitative XPS study of the surface films formed, by exposure to water, on Mg and on the Mg-Al intermetallics: Al_3Mg_2 and $Mg_{17}Al_{12}$", *Corrosion Science*, vol. 51, no. 5, pp. 1115–1127, 2009, ISSN: 0010-938X.

[18] S. Splinter, N. McIntyre, W. Lennard, K. Griffiths, and G. Palumbo, "An {aes} and {xps} study of the initial oxidation of polycrystalline magnesium with water vapour at room temperature", *Surface Science*, vol. 292, no. 12, pp. 130–144, 1993, ISSN: 0039-6028.

[19] A. Atrens, G.-L. Song, F. Cao, Z. Shi, and P. K. Bowen, "Advances in Mg corrosion and research suggestions", *Journal of Magnesium and Alloys*, vol. 1, no. 3, pp. 177–200, 2013, ISSN: 2213-9567.

[20] Z. Shi, F. Cao, G.-L. Song, and A. Atrens, "Low apparent valence of mg during corrosion", *Corrosion Science*, vol. 88, no. 0, pp. 434 –443, 2014, ISSN: 0010-938X.

[21] A. King, N. Birbilis, and J. Scully, "Accurate electrochemical measurement of magnesium corrosion rates; a combined impedance, mass-loss and hydrogen collection study", *Electrochimica Acta*, vol. 121, no. 0, pp. 394–406, 2014, ISSN: 0013-4686.

[22] S Mathieu, C Rapin, J Steinmetz, and P Steinmetz, "A corrosion study of the main constituent phases of AZ91 magnesium alloys", *Corrosion Science*, vol. 45, no. 12, pp. 2741–2755, 2003, ISSN: 0010-938X.

[23] M.-C. Zhao, M. Liu, G. Song, and A. Atrens, "Influence of the β-phase morphology on the corrosion of the mg alloy AZ91", *Corrosion Science*, vol. 50, no. 7, pp. 1939 –1953, 2008, ISSN: 0010-938X.

[24] W. Haynes, *CRC Handbook of Chemistry and Physics, 95th Edition*. CRC Press, 2014, ISBN: 1482208679.

[25] R. F. Egerton, *Physical Principles of Electron Microscopy*. Springer, 2005, ISBN: 0-387-25800-0.

[26] A. Rędzikowski. (Feb. 2013). Three-electrode setup for measurement of potential, [Online]. Available: {https://commons.wikimedia.org/wiki/File:Three_electrode (visited on 04/11/2015).

[27] M. P. Olson and W. R. Lacourse, "Analytical instrumentation handbook", in, 3rd ed. CRC Press, 2004, ch. Voltammetry, pp. 529–543.

[28] E. McCafferty, "Validation of corrosion rates measured by the tafel extrapolation method", *Corrosion Science*, vol. 47, no. 12, pp. 3202–3215, 2005, ISSN: 0010-938X.

[29] J. Hirmke, M.-X. Zhang, and D. StJohn, "Surface alloying of AZ91E alloy by Al-Zn packed powder diffusion coating", *Surface and Coatings Technology*, vol. 206, pp. 425–433, 2011, ISSN: 0257-8972.

[30] M. B. Kannan and W. Dietzel, "Pitting-induced hydrogen embrittlement of magnesium-aluminium alloy", *Materials and Design*, vol. 42, no. 0, pp. 321 –326, 2012, ISSN: 0261-3069.

[31] F Czerwinski, "The oxidation behaviour of an {az91d} magnesium alloy at high temperatures", *Acta Materialia*, vol. 50, no. 10, pp. 2639 –2654, 2002, ISSN: 1359-6454.

[32] A. Bakkar and V. Neubert, "Improving corrosion resistance of magnesium-based alloys by surface modification with hydrogen by electrochemical ion reduction (EIR) and by plasma immersion ion implantation (PIII)", *Corrosion Science*, vol. 47, no. 5, pp. 1211–1225, 2005, ISSN: 0010-938X.

[33] A. Pardo, M. Merino, A. Coy, R. Arrabal, F. Viejo, and E. Matykina, "Corrosion behaviour of magnesium/aluminium alloys in 3.5 wt.% NaCl", *Corrosion Science*, vol. 50, pp. 823–834, 3 2008, ISSN: 0010-938X.

[34] Q. Qu, J. Ma, L. Wang, L. Li, W. Bai, and Z. Ding, "Corrosion behaviour of AZ31B magnesium alloy in NaCl solutions saturated with CO_2", *Corrosion Science*, vol. 53, no. 4, pp. 1186–1193, 2011, ISSN: 0010-938X.

[35] M. Jönsson, "Atmospheric Corrosion of Magnesium alloys", PhD thesis, KTH Chemical Science and Engineering, 2007.